



ELSEVIER

Deep-Sea Research II 50 (2003) 3041–3064

DEEP-SEA RESEARCH
PART II

www.elsevier.com/locate/dsr2

A 1998–1992 comparison of inorganic carbon and its transport across 24.5°N in the Atlantic

A.M. Macdonald^{a,*}, M.O. Baringer^b, R. Wanninkhof^b, K. Lee^c, D.W.R. Wallace^d

^a *CIMAS, RSMAS, University of Miami, Miami, FL 33149, USA*

^b *NOAA/AOML/PHOD, 4301 Rickenbacker Csway, Key Biscayne, FL 33149, USA*

^c *School of Environmental Science and Engineering, Pohang Univ. of Science and Technology, San 31, Nam-gu, Hyoja-dong, Pohang 790-784, Republic of Korea*

^d *Forschungsbereich Biogeochemie Institut fuer Meereskunde an der Universitaet Kiel, Duesternbrooker Weg 20, Kiel D-24105, Germany*

Received 29 April 2002; received in revised form 17 April 2003; accepted 15 July 2003

Abstract

In January and February 1998, when an unprecedented fourth repetition of the zonal hydrographic transect at 24.5°N in the Atlantic was undertaken, carbon measurements were obtained for the second time in less than a decade. The field of total carbon along this section is compared to that provided by 1992 cruise which followed a similar path (albeit in a different season). Consistent with the increase in atmospheric carbon levels, an increase in anthropogenic carbon concentrations of $8 \pm 3 \mu\text{mol kg}^{-1}$ was found in the surface layers. Using an inverse analysis to determine estimates of absolute velocity, the flux of inorganic carbon across 24.5° is estimated to be -0.74 ± 0.91 and $-1.31 \pm 0.99 \text{ PgC yr}^{-1}$ southward in 1998 and 1992, respectively. Estimates of total inorganic carbon flux depend strongly upon the estimated mass transport, particularly of the Deep Western Boundary Current. The 1998 estimate reduces the large regional divergence in the meridional carbon transport suggested by previous studies and brings into question the idea that the tropical Atlantic constantly outgasses carbon, while the subpolar Atlantic sequesters it. Uncertainty in the carbon transports themselves, dominated by the uncertainty in the total mass transport estimates, are a hindrance to determining the “true” picture.

The flux of anthropogenic carbon ($C_{\text{★ANTH}}$) across the two transects is estimated as northward at 0.20 ± 0.08 and $0.17 \pm 0.06 \text{ PgC yr}^{-1}$ for the 1998 and 1992 sections, respectively. The net transport of $C_{\text{★ANTH}}$ across 24.5°N is strongly affected by the difference in concentrations between the northward flowing shallow Florida Current and the mass balancing, interior return flow. The net northward transport of $C_{\text{★ANTH}}$ is opposite the net flow of total carbon and suggests, as has been found by others, that the pre-industrial southward transport of carbon within the Atlantic was stronger than it is today. Combining these flux results with estimates of atmospheric and riverine inorganic carbon input, it is determined that today's oceanic carbon system differs from the pre-industrial system in that today there is an uptake of anthropogenic carbon to the south that is advected northward and stored within the North Atlantic basin. © 2003 Elsevier Ltd. All rights reserved.

*Corresponding author. WHOI Clark 3 MS21, 360 Woods Hole Road, Woods Hole, MA 02563, USA. Tel.: +1-508-289-3507; fax: +1-508-457-2181.

E-mail addresses: amacdonald@whoi.edu (A.M. Macdonald), molly.baringer@noaa.gov (M.O. Baringer), rik.wanninkhof@noaa.gov (R. Wanninkhof), ktl@postech.ac.kr (K. Lee), dwallace@ifm.uni-kiel.de (D.W.R. Wallace).

1. Introduction

Throughout the last decade approximately 6.2 PgC yr^{-1} ($1 \text{ PgC} = 1 \text{ GtC} = 10^{15} \text{ g}$ of carbon) have been released into the atmosphere through the burning of fossil fuels (IPCC, 2001; Battle et al., 2000). Meanwhile, the amount of carbon in the atmosphere has increased at a rate of only 2.8 PgC yr^{-1} ($1 \text{ PgC yr}^{-1} = 2642 \text{ kmolC s}^{-1}$). The increased partial pressure of atmospheric CO_2 has caused, through air–sea exchange, the amount of carbon stored in the ocean to increase by about $2.0 \pm 0.6 \text{ PgC yr}^{-1}$ (IPCC, 2001; Battle et al., 2000; Schimel et al., 1996; Siegenthaler and Sarmiento, 1993). These estimates strongly suggest that the ocean and ocean circulation are significant players in the global carbon cycle and control, in part, the rate of the atmospheric increase in CO_2 .

Just where the oceanic uptake of anthropogenic CO_2 is occurring and how circulation patterns affect the sources and sinks of carbon within the oceans are not well understood. Until recently direct oceanic observations have been sparse and numerical models, which have been extremely good at producing similar net ocean CO_2 storage estimates, have failed to produce a quantitative consensus on where the uptake and storage of anthropogenic carbon are occurring (Wallace, 2001; Orr et al., 2001). This study seeks to understand better one piece of this puzzle, that is the uptake and transport of carbon within the North Atlantic. We focus on the carbon transport across 24.5°N .

Previous estimates of the carbon transport across this line of latitude have been made. The earliest, Brewer et al. (1989) was based on carbon measurements taken at just nine stations occupied in the late fall of 1988, combined with the transport results of the full hydrographic transect made in 1981 (Hall and Bryden, 1982). The increased effort to measure carbon dioxide concentrations in seawater during the World Ocean Circulation Experiment (WOCE), the Ocean–Atmosphere Carbon Exchange Studies (OACES) and the US Joint Global Ocean Flux Study (JGOFS) programs has now provided us with a far more detailed view of the ocean carbon field. Rosón et al. (2002) presented inorganic carbon

and anthropogenic carbon transport estimates based on data from the summer 1992 occupation of the Atlantic 24.5°N transect. Their carbon transport estimates along with estimates from previous studies at other latitudes suggested that to the north of 24.5°N the subpolar ocean takes up carbon from the atmosphere, whereas to the south it is released to the atmosphere. We compare their data and results to those from the winter 1998 occupation of the 24.5°N transect, with particular emphasis on the carbon and anthropogenic carbon fields. Calculated meridional transport of inorganic and anthropogenic carbon allows us to provide an updated view of the uptake and storage within the Atlantic Basin.

2. The observations

In 1998, the R.V. Ronald Brown made a high density hydrographic transect across the North Atlantic at 24.5°N (Fig. 1 in black) sponsored by OACES. It was the second transect along this line of latitude to obtain measurements of carbon and carbon related species. The second leg of the cruise, which made these measurements left Las Palmas on January 23, 1998 and arrived in Charleston S.C. 1 month later on February 24. This leg included 130 CTD stations at which oxygen, nutrient and chlorofluorocarbon (CFC) measurements were taken with a 36 position bottle rosette. LADCP data also were obtained, but are not used in this particular study. Selected stations sampled dissolved organic carbon, dissolved inorganic carbon, alkalinity and pH. In this study, total inorganic carbon and total alkalinity were used in the determination of the 1998 pre-anthropogenic component of carbon (Chen and Millero, 1979; Gruber et al., 1996).

The 1998 cruise track was similar to that followed by the 1981 Atlantis cruise (AT109) in that it included a jog to the coast of Africa and sampled the Florida Straits at 27°N . In this study, the 1998 carbon data are compared to those collected in 1992 on the WOCE A5 transect undertaken by the R/V BIO Hespérides (Fig. 1 in red). This cruise track is similar to that of the 1957 IGY transect. It lies to the south of the 1998

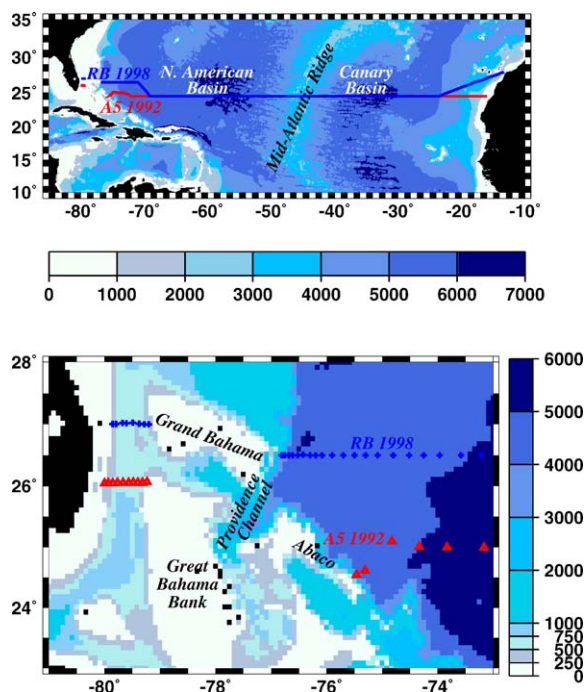


Fig. 1. Location of the stations for the 1998 (black and +) and 1992 (red and triangles) hydrographic stations. Note that the 1992 transect followed the path of the original 1957 IGY section, while the 1998 section follows more closely the path of the Atlantis 109 1981 section. Within the Florida Straits (lower panel) the 1992 data are from 26°N. The 1998 data are from 27°N. The more southerly crossing misses any flow that may pass through the Providence Channel.

track near both coasts and samples the Florida Straits at 26°N. Beginning on July 12, 1992 and ending on August 15, this earlier cruise occupied 112 CTD stations and used a 24-bottle rosette to provide measurements of oxygen, various nutrients, as well as alkalinity and pH, which were used to estimate total inorganic carbon, as few dissolved inorganic carbon measurements were made. The details of these data are given in Rosón et al. (2002). It should be noted that there has been a considerable effort within the community to produce a consistent set of reference standards for the carbon measurements. In their synthesis of Atlantic inorganic carbon data, Wanninkhof et al. (2003) found no consistent biases in O₂, TIC, or Talk among cruises.

The raw bottle data for both the 1998 and 1992 sections have been run through a standard

deviation check, and gaps have been filled using a multiparameter linear regression (MLR) technique (Holfort et al., 1998) where less than 50% of the data are missing from a cast. Otherwise, linear interpolation has been used. The cutoff on the use of the MLR preserved the character of the property profiles as in this particular instance, where only a single transect is used, the MLR technique tended to produce extremely noisy interpolated fields in the presence of large data gaps. The bottle data have been interpolated in neutral density space onto the CTD 2 db depths. In the deep basin, below 5000 db the interpolation is done in pressure space which allows better vertical resolution in more homogeneous waters.

To estimate anthropogenic CO₂ on the 24.5°N line, the so-called “ ΔC^{\star} ” method originally developed by Gruber et al. (1996) has been used. This method separates the anthropogenic CO₂ component (C^{\star}_{ANTH}) from the measured total inorganic carbon (TIC^{MEAS}) through three corrections: biology (ΔC^{BIO}), the carbon concentration that the water would have had at the surface in equilibrium with a pre-industrial atmospheric pCO₂ of 280 μatm (C^{EQ}), and the air–sea disequilibrium (ΔC^{DISEQ}).

$$C^{\star}_{\text{ANTH}} (\mu\text{mol kg}^{-1}) = \Delta C^{\star} - \Delta C^{\text{DISEQ}} \quad (1)$$

$$= \text{TIC}^{\text{MEAS}} - \Delta C^{\text{BIO}} - C^{\text{EQ}} - \Delta C^{\text{DISEQ}}. \quad (2)$$

The ΔC^{DISEQ} can be estimated using either the water mass information from transient tracers or the ΔC^{\star} distribution at depths thought to be unaffected by anthropogenic CO₂. For direct comparison to the previous study of the 1992 data set, we estimate C^{\star}_{ANTH} here using the method of Rosón et al. (2002), which differs from the one described above in that a constant disequilibrium value, ΔC^{DISEQ} , estimated from the ΔC^{\star} distribution in anthropogenic CO₂-free waters is applied to the entire water column. The disequilibrium term for the 1992 data set is $6.9 \pm 5 \mu\text{mol kg}^{-1}$ (Rosón et al., 2002) and $-11.1 \pm 2.0 \mu\text{mol kg}^{-1}$ for the 1998 data set. The former value is consistent with the $3.8 \pm 4.8 \mu\text{mol kg}^{-1}$ suggested by Pérez et al. (2002) for the eastern North Atlantic, while the

latter value is at the upper end of the -24 to $-10 \mu\text{mol kg}^{-1}$ range of Gruber (1998) for the North Atlantic. A more complete discussion of the anthropogenic carbon calculation is included in the appendix.

The resulting data set includes all available properties, as well as the derived $C_{\text{★ANTH}}$ estimates on 2 db pressure intervals. These data are used in a 1998–1992 comparison of the fields themselves and in a box inversion calculation of meridional property fluxes.

2.1. The carbon fields

To compare the data fields, the properties, already on the same vertical grid, were objectively mapped every 50 db onto the same horizontal grid: 0.5° in longitude, between 75.5°W and 16°W (Table 1). The technique used is similar to that described in Lavín (1999), which was in turn fashioned after Fukimori and Wunsch (1991). To handle the discontinuity created by the Mid-Atlantic ridge, below 2750 db the eastern and western basins were treated separately. The smoothing appears to work well everywhere, except within the abyss (below about 6000 m) where the lack of data produces large uncertainties.

2.1.1. Total inorganic carbon

Although differing somewhat in magnitude, at 24.5°N in the Atlantic, the 1998 and 1992 TIC (total inorganic carbon) fields display similar features (Fig. 2, upper panels). Carbon concentrations increase from the surface to depth. They are greater in the east than in the west. Near the surface the lower CO_2 concentrations towards the west are associated with warmer temperatures. Using the 1998 field by way of example, it can be seen that although the top to bottom difference in carbon concentration is only $\text{O}(280 \mu\text{mol kg}^{-1})$ compared to a mean of $\text{O}(2100 \mu\text{mol kg}^{-1})$, the strongest vertical gradients are confined, as expected, to the waters above 1000 m. Below 1000 m, the range in concentrations is less than $60 \mu\text{mol kg}^{-1}$.

There is a relative maximum in TIC at ~ 1000 db in the eastern basin associated with

Table 1

To perform the objective mapping of the property fields every 50 db throughout the water column an estimate was made, from the data itself, of signal variance, eddy variance and intrinsic (or measurement) variance according to the assumptions about length scales given above

Objective mapping details

Signal covariance	Efolding scale of 400 km 200 km in deep basins
Eddy noise	Decorrelation length scale 175 km
Intrinsic noise	Uniform variance Uncorrelated over mean station separation

Analysis of the interpolation error was performed according to Bretherton et al. (1976).

the Mediterranean outflow. The weaker maximum in the west at the same depth is identified with the CFC minimum of Upper Circumpolar Deep Water (UCDW). Antarctic Intermediate Water (AAIW) lies above at about 850 db. The TIC minimum which appears to emanate from the western side of the basin encompasses both the Upper and Middle North Atlantic Deep Water (NADW) water masses. These include upper and classical LSW which appear as a single water mass (1200–2300 db) in the 1998 section, the CFC minimum of Iceland–Scotland Overflow Water (at ~ 2500 db), down to about 3400 db just above the core of Lower NADW recognized by its CFC maximum. In the abyss, particularly in the western basin, higher concentrations are associated with Antarctic Bottom Water.

The largest uncertainties in the interpolation (Fig. 2, lower left panel) occur in the regions of the strongest gradients. In the 1998 transect this is at about 100 m. In the 1992 transect, the uncertainty remains high above 100 m all the way to the surface as the concentration gradients are stronger in the near surface waters during the summer.

Using the estimated errors from the two TIC fields to determine the uncertainty in the differenced fields, it was found that the apparent differences between the 1992 and 1998 TIC concentrations (Fig. 2, lower right panel) were not significant at individual grid points. However, there are clearly patterns within the field. Since it is

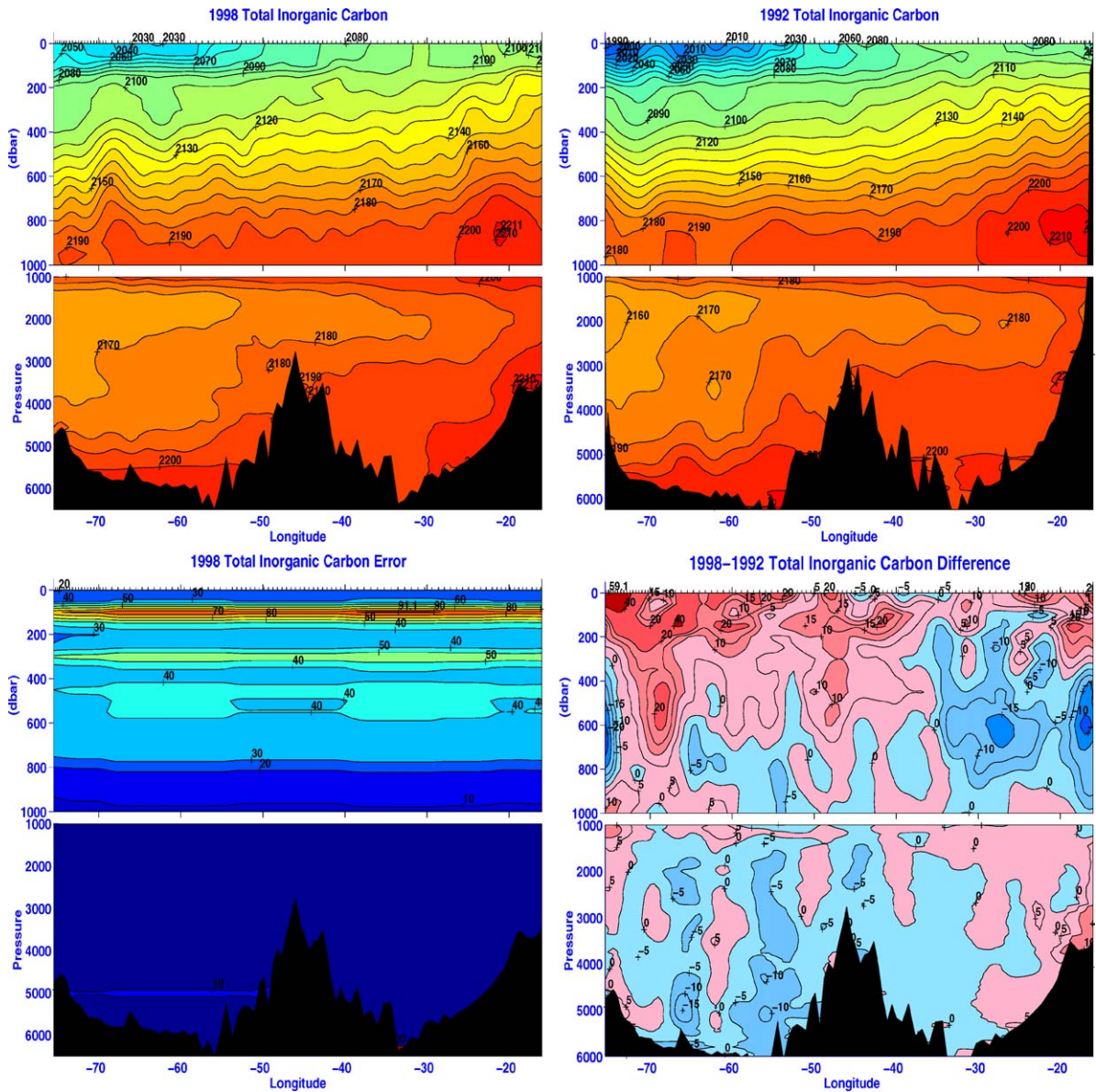


Fig. 2. The 1998 (upper left panel) and 1992 (upper right panel) objectively mapped fields of total dissolved inorganic carbon (CI = [1920 : 10 : 2250]). The 1σ standard deviation (interpolation error) field for the 1998 TIC field (lower left panel, CI = [0 : 10 : 100]) and the 1992 TIC field subtracted from 1998 TIC field (lower right panel, CI = [-40 : -20 : 5 : 20 : 40]). In the difference field pink shading indicates an increase over time, blue, a decrease. Units are μmol kg⁻¹. The tick marks along the upper borders of the plots indicate station location.

likely that both properties and property differences are correlated across individual measurements, and such correlations would reduce the error, averaging was invoked. Zonal averaging of

these data indicates that there was a significant increase in TIC concentrations in the upper layers over the 6-year period. This increase is a maximum at the surface, ($\sim 14 \pm 7 \mu\text{mol kg}^{-1}$, where the

uncertainty is the square root of the variance in the surface layer), falls off to zero by 600 m, and the pattern (Fig. 2) indicates that the increase is strongest in western basin near the recirculation region (70°W). Removing some of the differences associated with evaporation and precipitation through a normalization to a standard salinity, $S = 35$ ($NTIC = TIC \cdot S / 35$), the surface increase from 1992 to 1998 is estimated at $8 \pm 6 \mu\text{mol kg}^{-1}$. Both TIC and especially NTIC are well correlated across the basin with the seasonal decrease in temperature. Although the apparent increase in carbon concentrations in the LSW and AABW near the western boundary (70–80°W) should be noted, they do not represent enough of a pattern to be considered significant compared to the noise level.

2.1.2. Anthropogenic carbon

Anthropogenic carbon ($C \star_{\text{ANTH}}$) has been calculated in a similar fashion for both the 1998 and 1992 sections (Fig. 3, upper panels). As expected, higher values of $C \star_{\text{ANTH}}$ are associated with more recently ventilated waters. There is a maximum from the surface to about 200 m depending upon longitude, and a decrease in $C \star_{\text{ANTH}}$ concentrations with depth. The highest concentrations occur at the surface in the eastern portion of the basin. Between 20°W and 70°W the average mixed-layer concentration of $C \star_{\text{ANTH}}$ decreases by about $0.5 \mu\text{mol kg}^{-1}$ for every degree of longitude. At 70°W the average mixed-layer concentration is 45 ± 5 and $51 \pm 3 \mu\text{mol kg}^{-1}$ for the 1992 and 1998 transects, respectively. The mean mixed layer concentrations in the Florida Straits are higher: $52 \pm 5 \mu\text{mol kg}^{-1}$ in 1992 and $70 \pm 2 \mu\text{mol kg}^{-1}$ in 1998. In the western basin there is a slight maximum in $C \star_{\text{ANTH}}$ associated with the chlorofluorocarbon (CFC) maximum of LSW (Fig. 4, ~1500 db). Zonal averaging (Fig. 5) of the data suggests a change in the vertical gradient of $C \star_{\text{ANTH}}$ associated with a similar CFC feature at the depth of UCDW/AAIW interface at ~800 db.

We look to chlorofluorocarbons whose spatial and temporal variations have been previously scrutinized (e.g. Beining and Roether, 1996; Warner et al., 1996; Doney et al., 1998;

Mecking, 2001) to understand better some of the features in the $C \star_{\text{ANTH}}$ fields. The 24.5°N sections of CFC11 and CFC12 are similar. Here, we concentrate on the CFC12 fields as the atmospheric partial pressure of this tracer has continued to rise over recent years, whereas CFC11 partial pressures have begun to decline, therefore CFC12 provides better diagnostics of recent water mass ventilation. CFC12 concentrations are relatively high near the surface and there are maxima at about 150–200 m and at 1500 m (Fig. 4, left panel). The former appears to emanate from the surface layers near the eastern boundary (which are also rich in $C \star_{\text{ANTH}}$), but is seen across the entire basin. The latter is mainly in the western boundary (LSW) (Molinari et al., 1998).

Using equilibrium CFC partial pressures ($p\text{CFC} = \text{measured CFC concentration} \cdot \text{CFC solubility function}$ (Warner et al., 1996)) to remove most of the differences due to temperature variations (Fig. 4, right panel), it is found that due to greater solubility at lower temperatures, the 200-m CFC maximum does not appear in the $p\text{CFC}$ field so the largest signal in $p\text{CFC}12$ is at the surface. Its disappearance suggests that this upper layer signal is seasonal in origin. This hypothesis is consistent with the findings of Doney and Bullister (1992) that a subtropical North Atlantic maximum in CFCs at depths of 100 to 200 m along a meridional line at about 20°W is caused by the sensitivity of CFC solubility to temperature, and heating and degassing of the seasonal thermocline.

The $C \star_{\text{ANTH}}$ maximum at 200 m is either an artifact of the calculations due to remineralization ratios in the top of the thermocline that do not follow Redfield stoichiometry or it is caused by the capping of the winter mixed layer by the seasonal mixed layer containing lower concentrations of $C \star_{\text{ANTH}}$. Apparent oxygen utilization in the top 100 m of the 1998 data set is $-4 \pm 6 \mu\text{mol kg}^{-1}$, therefore a small overestimate on $C \star_{\text{ANTH}}$ of order $3 \mu\text{mol kg}^{-1}$ is possible due to oxygen oversaturation. In either case, these anomalies appear to cause relatively little bias in the section-wide integral of $C \star_{\text{ANTH}}$ transport outside the 200 m depth range (Fig. 5).

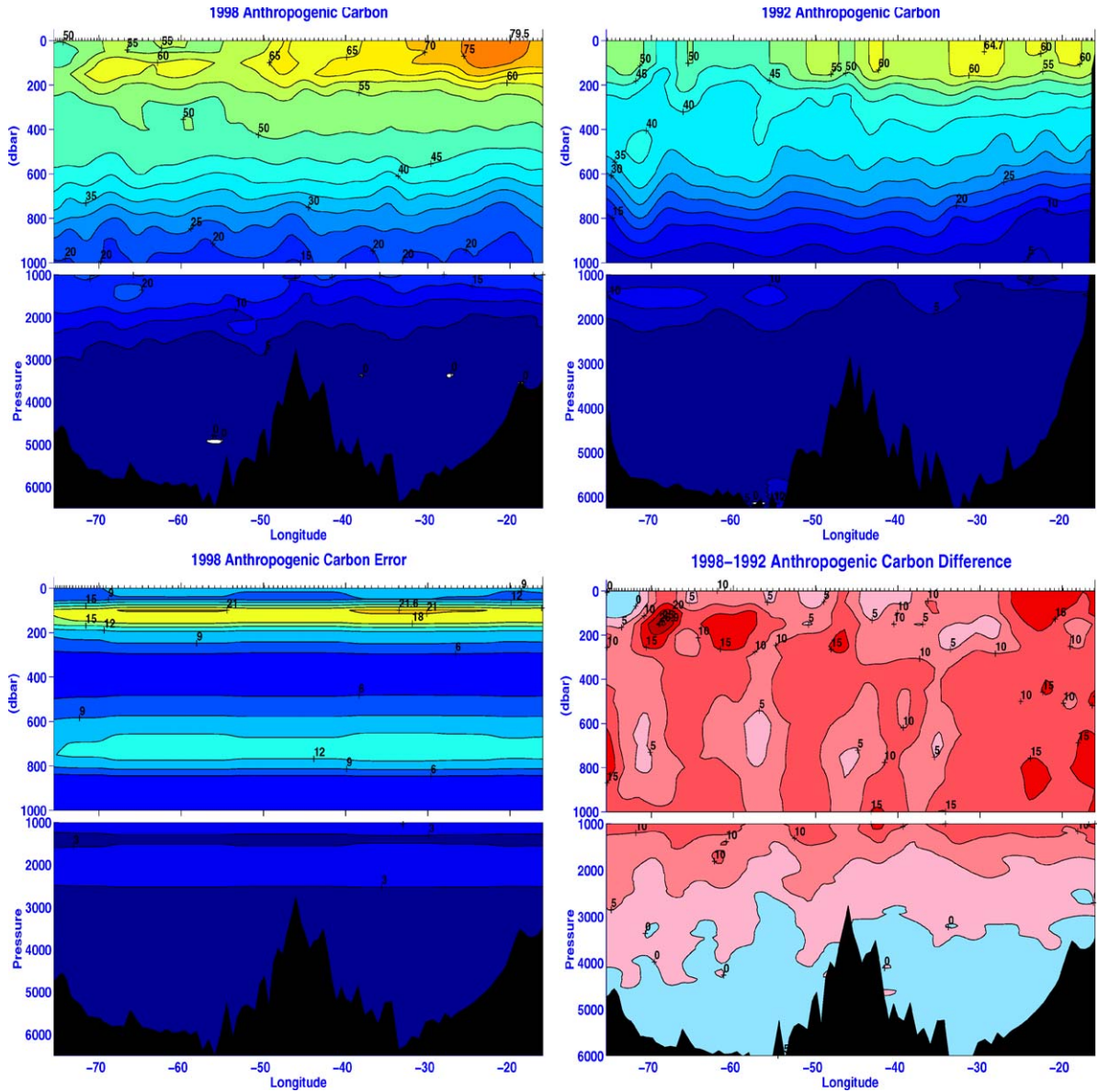


Fig. 3. The 1998 (upper left panel) and 1992 (upper right panel) objectively mapped fields of anthropogenic carbon ($C_{★ANTH}$, $CI = [0 : 5 : 100]$). The 1σ standard deviation (interpolation error) field for the 1998 $C_{★ANTH}$ field (lower left panel, $CI = [0 : 3 : 30]$) and the 1992 $C_{★ANTH}$ field subtracted from 1998 $C_{★ANTH}$ field (lower right panel, $CI = [-25 : 5 : 25]$). In the difference field pink shading indicates an increase over time, blue, a decrease. Units are $\mu\text{mol kg}^{-1}$. The tick marks along the upper borders of the plots indicate station location.

The estimate of $C_{★ANTH}$ assumes stationarity and that increases in dissolved inorganic carbon due to organic carbon remineralization is in fixed stoichiometry with increases in nitrate (see the appendix). Although these assumptions may not

hold strictly, particularly on longer timescales, they are reasonable assumptions for the present comparison. Recent basin-wide $C_{★ANTH}$ calculations (Sabine et al., 1999, 2002) suggest estimation uncertainties of order $5 \mu\text{mol kg}^{-1}$ above 1500 m

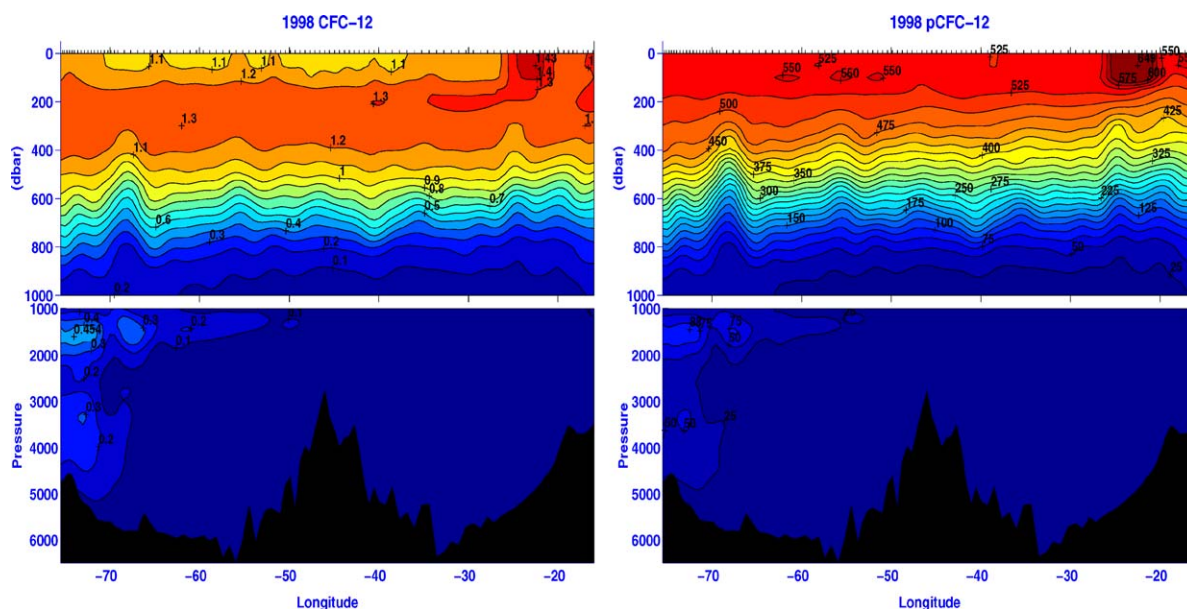


Fig. 4. The 1998 fields of CFC-12 (left hand panel) and pCFC-12 (right hand panel). Units are ppt.

and $3.5 \mu\text{mol kg}^{-1}$ below this level. Therefore, it is reasonable to use $C \star_{\text{ANTH}}$, which is after all the perturbation signal in which we are interested, to examine changes in carbon concentrations over time. As with TIC, although most of individual mapped features are not significant, there is a pattern to the differences between the 1998 and 1992 $C \star_{\text{ANTH}}$ fields (Fig. 3, lower right panel). The magnitude of the changes are of the order of $10 \mu\text{mol kg}^{-1}$.

Assuming that the surface water increase keeps pace with the atmospheric CO_2 rise, estimates of p CO_2 along the 24°N line (calculated according to Lewis and Wallace (1998) from measured alkalinity, TIC and temperature along with the atmospheric CO_2 increase from 1992 to 1998) suggest an increase in surface water TIC of about $7 \mu\text{mol kg}^{-1}$ between 1992 and 1998. This value compares well to other recent, but less local estimates, $6 \mu\text{mol kg}^{-1}$ (Lee et al., 2000a) and $10 \mu\text{mol kg}^{-1}$ (Bates et al., 1996). Consistent with these estimates and our own estimate of surface changes in TIC and NTIC, horizontal averaging across the basin reveals a surface increase in $C \star_{\text{ANTH}}$ from 1992 to 1998 of $8 \pm 3 \mu\text{mol kg}^{-1}$. The maximum increase occurs from about

150–200 m. Increases of the order of $10 \mu\text{mol kg}^{-1}$ are apparent to about 1000 m and horizontally averaging deeper layers we find increases greater than $5 \mu\text{mol kg}^{-1}$ down to 2000 m. These increases are concentrated near the western boundary in the DWBC and suggest an important role for this current in moving ocean $C \star_{\text{ANTH}}$ away from the ventilation regions to the north. Below 3000 m in the eastern basin and 4000 m in the western basin, the suggested decrease in $C \star_{\text{ANTH}}$, is the same order or smaller than the uncertainty in the estimation, and is therefore not significant.

Turning again to the equilibrium CFC partial pressures, we find some similarities in the types of changes which have occurred. Between 1992 and 1998 there has been an overall increase of pCFC12 with time. In the zonal average (Fig. 5) there is a large maximum (70 ppt) at 500 m and another, lesser maximum at 1500–1800 m. The shallower maximum is greatest in the western boundary in the 200 m to 800 m range, comprised of the relatively well ventilated water masses of AAIW and UCDW. It is also evident across the entire extent of the basin. The deeper maximum is confined to the western side of the western basin in the region of LSW.

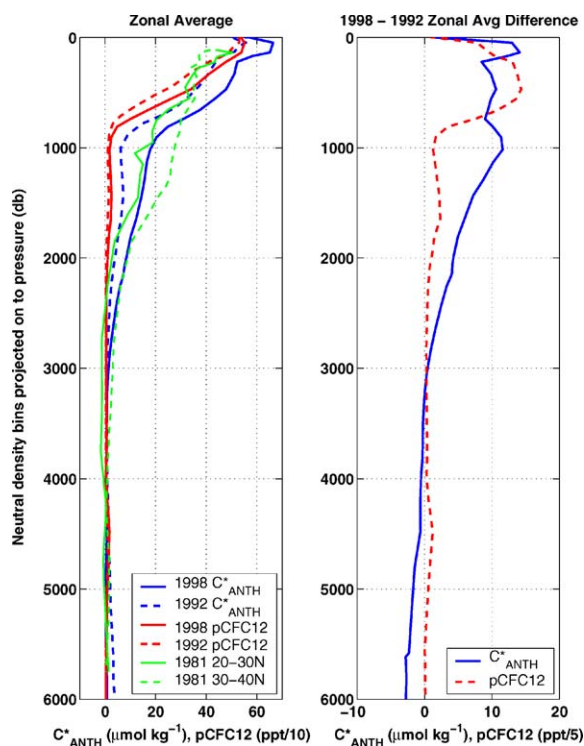


Fig. 5. Comparison of the zonal average C^*_{ANTH} and pCFC12 concentrations. Left hand panel illustrates the vertical distribution of the two properties for both 1998 and 1992. The right hand panel shows the difference between the 1998 and 1992 profiles for each of the properties. The 1981 anthropogenic carbon curves (labeled 20–30N and 30–40N) are data averaged between the specified latitudes and are from Gruber (1998).

To summarize, differences in both TIC and C^*_{ANTH} over the 6-year period between 1992 and 1998 suggest an increase in carbon concentrations in the upper layers with a near-surface maximum. The increase of both properties in the surface layers is consistent with the changes occurring in the atmosphere. The enhancement in concentrations appears to go deeper than just the surface layers with the deep changes concentrated in the far western basin. The increase in C^*_{ANTH} that we take to be significant to about 2000 db is consistent with the increase in pCFC12 (Fig. 5). However, the spatial pattern of the increases are somewhat different. The increase in pCFC12 displays a sharp reduction between 500 and 1000 m, whereas the increase in C^*_{ANTH} concentrations displays a much more gradual gradient

with depth. Gruber (1998) averaged concentrations of anthropogenic carbon for the latitude bands 20–30°N and 30–40°N using data taken from the Transient Tracers in the Ocean North Atlantic Study program 1981. Comparing these profiles to those at 24.5°N (Fig. 5) suggests that the profile of C^*_{ANTH} at 24.5°N, even at depth, is moving towards the higher values previously associated with waters lying further to the north (also see Gruber, 1998, Figs. 8c and d).

It should be noted that the C^*_{ANTH} difference fields may still contain biases or systematic errors in spite of the care taken on our part to calculate this derived variable for the 1998 data set in a fashion similar to that used for the 1992 data set. One such source of error may arise from the fact that the 1998 TIC values were measured whereas the 1992 values were calculated from measured pH and total alkalinity, and although the TIC values for these two data sets have been closely compared to remove biases as part of the Atlantic synthesis effort (Wanninkhof et al., 2003), there is still the possibility of errors which change with depth.

3. Carbon transport

3.1. Method

To obtain an estimate of the absolute meridional velocity field for each of the two 24.5°N transects a simple inverse box model has been used. It is based upon the same box inverse model method introduced to the physical oceanographic community by Wunsch (1978) and later described in much greater detail in Wunsch (1996). The inverse method as used here is simply a technique for estimating ocean circulation based on hydrographic observations and a set of simple physical constraints. The observations (temperature and salinity) allow for the calculation of geostrophic velocities relative to a reference surface. The model physics (in this case a set of conservation equations) is used to constrain the possible solutions for the unknown velocities at the reference surface in a least-squares sense. The model software originates from the system created

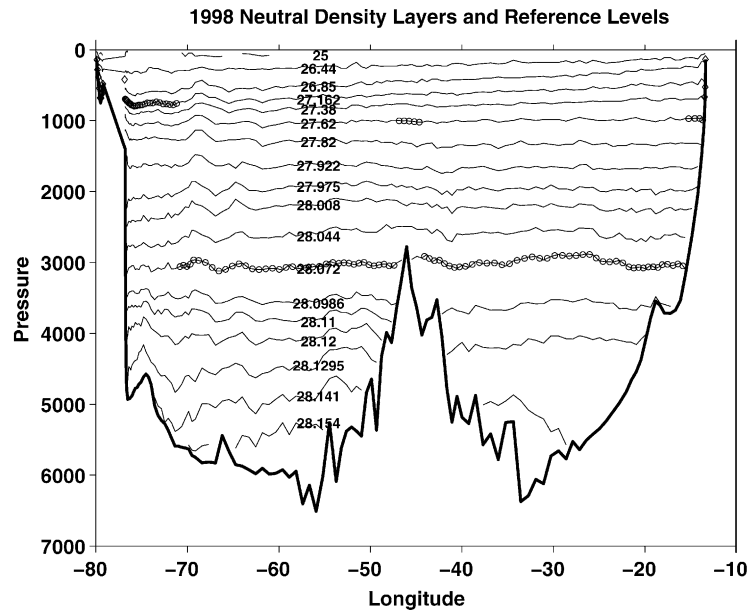


Fig. 6. Neutral density surfaces used to create the layers for the 1998 transect inverse models. Shown as diamonds and circles are the velocity reference levels for the transect. The circles represent the neutral density surface (28.072) just below 3000 db across most of the section and surfaces higher in the water column in the region of the DWBC and the Mid-Atlantic Ridge. The diamonds indicate station pairs at which the specified reference levels are deeper than the bottom, in which case the deepest common level is used. The inverse model determines the velocities for these reference levels that are consistent with the model physics and constraints. The 1992 model uses the same neutral density layer interfaces and a similar set of velocity reference levels.

by P. Robbins, J. Toole, G. Johnson and S. Wijffels to examine Pacific circulation.

The models are defined by 21 neutral density (σ) interfaces in the vertical (Fig. 6) and the observed station spacing in the horizontal. The flow is assumed to be hydrostatic and geostrophic so that the thermal wind equations apply. Relative geostrophic velocities are computed between stations pairs on the CTD 2-dbar pressure intervals and are integrated vertically to produce layer transport equations. The models are made up a set of transport constraint equations of the following form.

$$\begin{aligned} & \sum_i \sum_j \rho_{ij} \mathbf{a}_{ij} \mathbf{v}_{iU} C_{ij} - Ek_c \sum_i \sum_k \rho_{ik} \mathbf{a}_{ik} C_{ik} \mathbf{v}_{ikEK} \\ & \approx - \sum_i \sum_j \rho_{ij} \mathbf{a}_{ij} \mathbf{v}_{ijR} C_{ij} \\ & + \sum_i \sum_k \rho_{ik} \mathbf{a}_{ik} C_{ik} \mathbf{v}_{ikEK} \\ & + \text{known flux into or out of a box } \dots, \quad (3) \end{aligned}$$

where i, j, k are the station pair, layer and Ekman layer indices; ρ the density; \mathbf{v}_R the relative velocity; \mathbf{v}_U the unknown reference level velocity; \mathbf{v}_{EK} the initial Ekman velocity estimate; \mathbf{C} the property concentration; \mathbf{a} the vertical layer area; Ek_c the multiplicative Ekman component correction factor.

These equations are combined to form the familiar constraint set $\mathbf{A}\mathbf{b} + \mathbf{n} = \mathbf{y}$, where, the elements of the \mathbf{A} matrix are $A_{ij} = \int_B^T \rho_{ij} \mathbf{a}_{ij} C_{ij} dp$ and are constructed from the integrated CTD pressure values. T and B are the top and bottom pressures, respectively, of the layer or sets of layers used in an individual constraint. The vector \mathbf{b} represents the unknown reference level velocities (\mathbf{v}_U) resulting from the dynamic method and the correction terms to the initial Ekman estimates. The right-hand side vector, \mathbf{y} contains the known relative velocity transports and can include Ekman transport, and freshwater inflow/outflow and other net transport estimates.

The constraints are based upon the baroclinic flow field described by the hydrographic transects,

initial order of magnitude estimates of velocity at the reference surface, and estimates of the solution and data covariances. Since these constraints (Eq. (3)) are based on the flux across the sections only, the equations for our models are particularly simple and do not include diapycnal transfer or diffusion terms. The models presented here begin with initial estimates of net mass transport (entering from the north through the Bering Straits), net surface freshwater input from evaporation minus precipitation and rivers, and Ekman transport (Table 2).

The initial uncertainty estimate of $2 \times 10^9 \text{ kg s}^{-1}$ in the top to bottom mass transport constraint has been computed in the following manner: (1) The uncertainty on the flow through the Bering Strait ($0.3\text{--}0.6 \times 10^9 \text{ kg s}^{-1}$) (Coachman and Aagaard, 1988; Roach et al., 1995). (2) The uncertainty in the wind field (20% or $1.1 \times 10^9 \text{ kg s}^{-1}$) comes from the range suggested by various wind products (Hellerman and Rosenstein (1983), the Southampton Oceanography Centre global wind stress climatology, and the NCEP-NCAR and ECMWF atmospheric reanalyses). The Hellerman and Rosenstein (1983) field was used in the model because its net Ekman transport was closest to the mean of these four products. The 20% uncertainty is consistent with the low end of the range suggest by Ganachaud and Wunsch (2003). (3) The

uncertainty in the baroclinic variability taken to be order ($1 \times 10^9 \text{ kg s}^{-1}$), which is low compared to the 5 Sv suggested by Ganachaud and Wunsch (2003). (4) The uncertainty due to measurement noise is taken as $1 \times 10^9 \text{ kg s}^{-1}$, again low compared to the 3 Sv suggested by Ganachaud and Wunsch (2003) for mid-latitudes where it is dominated by vertical heave of density surfaces by internal waves. (5) The uncertainty due to unobserved bottom triangle transport is taken to be $O(1 \times 10^9 \text{ kg s}^{-1})$ the same as that suggested by Ganachaud and Wunsch (2003). (6) The uncertainty in the evaporation minus precipitation plus river runoff to the north of the transects is taken conservatively as 30% or $0.2 \times 10^9 \text{ kg s}^{-1}$. (7) We assume that the error due to unobserved ageostrophic motions (e.g., inertial oscillations) is negligible. The net uncertainty arising from (1)–(7), assuming that they are independent of one another, is $2.08 \times 10^9 \text{ kg s}^{-1}$, which has been rounded off to $2 \times 10^9 \text{ kg s}^{-1}$. It should be considered an optimistic estimate of the net uncertainty in the top to bottom mass flux.

Although other constraints such as silica conservation have been tested, the models used here are based solely on top-to-bottom mass and salt conservation. A constraint on the expected transport in the Florida Strait is also included (Table 2). The layer interfaces for the model were based upon

Table 2

Inverse model constraints, a priori estimates of uncertainty, data sources, and a priori estimates of solution variance

Basic model constraints

Mass flux

Geostrophic + Ekman flux^a = freshwater flux^b with an

integration reference point at Bering Strait^c $-0.78 \pm 2 \times 10^9 \text{ kg s}^{-1}$

Salt flux

Geostrophic + Ekman flux^a = Bering Strait transport^c $-27.7 \pm 20 \times 10^6 \text{ kg s}^{-1}$

1992

Total transport in the Florida Straits at 26°N: $30 \pm 1.0 \times 10^9 \text{ kg s}^{-1}$

1998

Total transport in the Florida Straits at 27°N: $32 \pm 1.0 \times 10^9 \text{ kg s}^{-1}$

Initial magnitude of unknowns

20–30 cm s^{-1}

Reference level velocities in Florida Straits

2 cm s^{-1}

Reference level velocities in the interior

6 cm s^{-1}

Reference level velocities where reference level is the bottom

20%

Correction factor to input Ekman flux

Ekman fluxes are computed from annual mean winds.

^a 1992 Ekman flux: Hellerman and Rosenstein (1983), $5.75 \times 10^9 \text{ kg s}^{-1} \pm 20\%$ and 1998 Ekman flux: Hellerman and Rosenstein (1983), $5.60 \times 10^9 \text{ kg s}^{-1} \pm 20\%$.

^b Freshwater flux: Schmitt et al. (1989), $0.07 \times 10^9 \text{ kg s}^{-1} \pm 30\%$.

^c Bering Strait: Roach et al. (1995) $0.83 \pm 0.66 \times 10^6 \text{ m}^3 \text{ s}^{-1}$ at -1°C and $S = 32.5$.

the work of Ganachaud (1999), which in turn was based on Macdonald (1998) and Rintoul and Wunsch (1991). The reference levels are based on Rintoul and Wunsch (1991) and Lavín (1999), which showed that the use of a reference surface across the interior basin of about 3000 db leads to more realistic deep property balances. We have chosen to raise the reference surface out of the DWBC to approximately 800 db (where the Abaco moorings show an average 0 velocity) and in regions where it runs into topography near the coasts. Tests have been performed on a variety of reference surface choices besides those indicated in Fig. 6. In particular, a shallow set on $\Gamma = 27.38$ (~ 800 db) in the western basin and $\Gamma = 27.62$ (~ 1000 db) in the eastern basin and a deep set on $\Gamma = 28.072$ (~ 3000 db) were tested. The results of these runs will be mentioned where relevant. Solutions (i.e. estimates of velocities at the reference surface and corrections to the initial Ekman component estimates) are found using a tapered-weighted least-squares (Gauss–Markov type) technique (Wunsch, 1996; Macdonald, 1998). This technique weights the system only by a priori estimates of the data and solution covariance.

3.2. Meridional mass transport across 24.5°N

The models have little trouble in meeting the constraints as long as large enough reference velocities are allowed for in the Florida Straits (see Table 2). This result is to be expected as the system is extremely under-determined. Larger reference velocity adjustments were required everywhere for the 1992 section, for, as will be shown shortly, the initial imbalance was larger. The shapes of the reference level velocity curves (Fig. 7) follow the changes in the initial estimate of the magnitude of the solutions. The solution size also follows the shape of the bathymetry. Because this system has been solved using a Gauss–Markov-type formulation, there has been no attempt to weight or scale the constraints or unknowns by anything other than the initial estimates of data and solution covariance (Wunsch, 1996). That is, there has been no attempt to remove the effects of differences in bottom

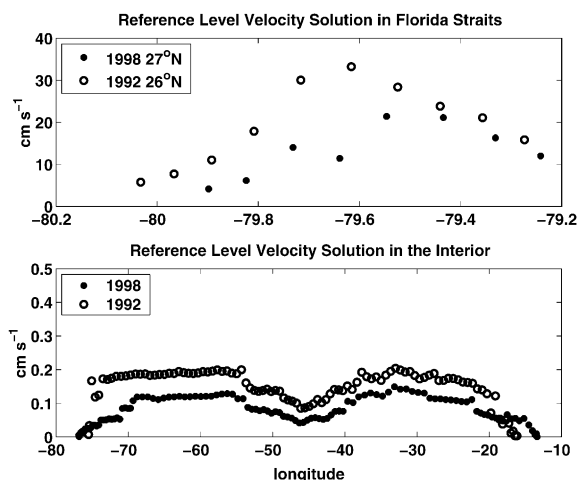


Fig. 7. The velocity solutions for the 1998 and 1992 transects for the reference levels shown in Fig. 6.

depth, station spacing, etc. The corrections to the initial estimates of Ekman transport were minute as would be expected given the simplicity of the model.

The model produces circulation patterns (Figs. 8 and 9) based on the initial constraints and assumptions. The initial imbalances are large because Florida Current transport is under-estimated by the initial guess. To meet the constraints, the mass transport through the Florida Straits is increased by 6.5×10^9 and 9.4×10^9 kg s^{-1} in the 1998 and 1992 transects, respectively. Over the interior a fairly uniform decrease in the southward transport (Fig. 8, upper panels) has occurred throughout most of the water column. An increase in northward transport of bottom water is also apparent. (Note the definition of which layers we include in our use of the terms surface, intermediate, deep and bottom waters are given in Table 3).

Zonally integrated solutions for the models using the deep and shallow reference surfaces mentioned earlier are not significantly different from those shown here. However, locally specific differences in the resulting circulation patterns for these test models led us to the reference surfaces chosen for the final models. For instance, the model with the deep 3000 m reference level, which began with an initial imbalance of less than

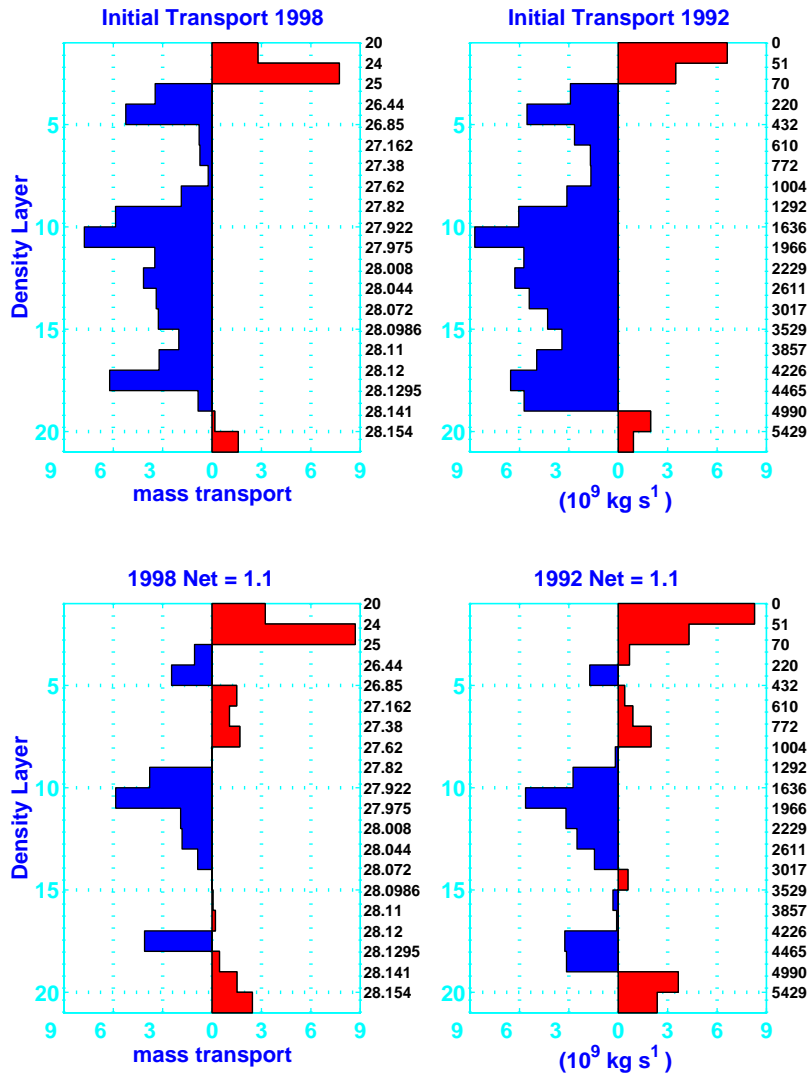


Fig. 8. Upper panels: the initial meridional transport profiles based on zero velocity at the reference levels (Fig. 6) for the 1998 (left-hand side) and 1992 (right-hand side) 24.5° Atlantic transects. Lower panels: the same, showing the final transport profiles based on the model estimates of the velocity at the reference levels (Fig. 7). The right axis of the left hand panels indicates the neutral density of each layer interface. The right axis of the right-hand panels indicates the average pressure of the layer interfaces in dbar. The net values given at the top of the lower panels is the net transport integrated from top to bottom. Positive values indicate northward flow.

$6 \times 10^9 \text{ kg s}^{-1}$ for both sections, could not produce a significant deep western boundary current (DWBC), and in fact, produced northward transport of these waters in the 1992 model. It also produced a strong deep southward transport ($\sim -16 \times 10^9 \text{ kg s}^{-1}$) in the far eastern basin, which we had no reason to expect. The shallow model, which had no trouble producing recogniz-

able DWBCs, produced no net transport of bottom water in the 1992 section and large variations in deep water transport across the basin in both sections.

Integrating from the coast east to 70°W to include local recirculation, the present model estimates the DWBC transport to be $-43 \pm 21 \times 10^9$ and $-43 \pm 25 \times 10^9 \text{ kg s}^{-1}$ for the 1998 and

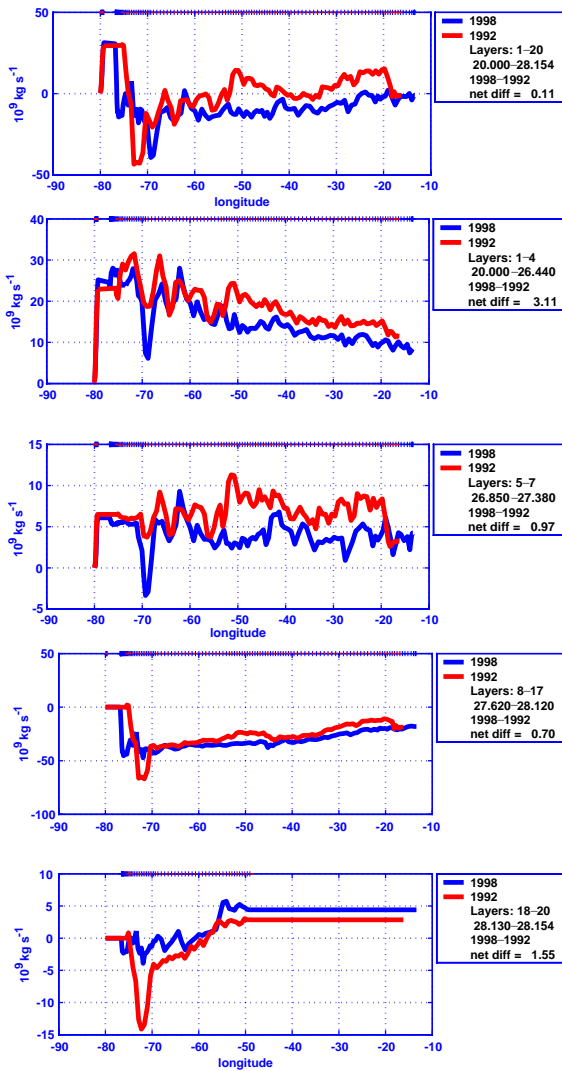


Fig. 9. A comparison of the integrated absolute mass transport (including Ekman flow) for the 1998 (dark/blue) and 1992 (light/red) transects. The boxes to the right indicate the neutral density layers included in the integration (see Fig. 6), the difference in net transport between the two transects and the direction of the subtraction. The integration is performed from west to east. The lines at the top indicate the availability of data within the layer set for each station pair. Positive values indicate northward flow.

1992 transects, respectively. These estimates are well within the mean and standard deviation ($-40 \pm 13 \times 10^6 \text{ m}^3 \text{ s}^{-1}$) suggested by Lee et al. (1996) from their 4.7-year time series. The

Table 3
Summary of Atlantic 24°N mass transport

Atlantic 24°N meridional mass transport (10^9 kg s^{-1})				
Layer type	Model layers	Fl. St.	Interior	Total
1992				
Top to bottom	1–20	29.5 ± 1.0	-30.6 ± 1.4	-1.1 ± 1.0
Surface	1–4	22.9 ± 0.8	-11.4 ± 1.7	11.5 ± 1.8
Intermediate	5–7	6.5 ± 0.7	-3.2 ± 2.3	3.3 ± 2.4
Deep	8–17	0.8 ± 0.1	-18.8 ± 4.0	-18.8 ± 4.0
Bottom	18–20		2.9 ± 3.5	2.9 ± 3.5
1998				
Top to bottom	1–20	31.4 ± 1.0	-32.3 ± 1.3	-1.0 ± 0.9
Surface	1–4	25.2 ± 0.7	-16.8 ± 1.6	8.4 ± 1.7
Intermediate	5–7	6.1 ± 0.5	-1.9 ± 2.7	4.2 ± 2.7
Deep	8–17	0.1 ± 0.1	-18.1 ± 4.5	-18.1 ± 4.5
Bottom	18–20		4.4 ± 3.6	4.4 ± 3.6

Note the 1992 model has an initial estimate of Florida Strait mass transport which was $2 \times 10^9 \text{ kg s}^{-1}$ less than what was used in the 1998 model to account for the flow through the Providence Channel missed by the 26°N Florida Strait measurements. Positive values indicate northward flow.

uncertainties encompass the range of transport estimates obtainable using different limits of integration. The DWBC position and magnitude is extremely variable (Lee et al., 1996; Fillenbaum et al., 1997), and it should be noted that the 1998 measurements were taken 2° farther north than the 1992 measurements and had better resolution, i.e. shorter distance between stations (Fig. 1). Nevertheless, both transects were able to capture a representative portion of the DWBC transport. Integrating the 1992 data from the coast to the point of maximum transport produces an estimate of $-82 \pm 22 \times 10^9 \text{ kg s}^{-1}$ (Fig. 9, panels 3 and 4). This number includes, however, recirculating transport associated with the offshore eddy, which appears to be much stronger and deeper in the water column in 1992 than in 1998.

In general, the transport in the two sections are similar both in the vertical and in the horizontal. Some of the differences include: a southward transport in the intermediate waters (Fig. 9, panel 3) in 1998, where northward transport occurs in 1992; a compensating, strong, intermediate, southward transport in the far, eastern 1992 basin; a stronger, surface intensified offshore eddy in 1998

(there appears to be no net mass transport associated with this feature in either section); and a stronger and deeper 1992 bottom transport (Fig. 8). Both transects have a small southward transport in the near surface layers, and slight northward transport between about 3000 and 3500 db (1992) and 3800–4200 db (1998).

Neither of these last two features are seen in the calculation of Lavin et al. (2003), which used the 1992 data set, similar, but not identical reference surfaces and a different technique for computing the absolute circulation field. They were not seen in the Roemmich and Wunsch (1985) analysis of the 1981 transect using an initial reference surface of $\sigma_2 = 36.8$ (~ 1300 m), but they were seen in their analysis of the 1957 IGY transect. They are also seen in the Rintoul and Wunsch (1991) re-analysis of the 1981 data set, which used a 3000 db initial reference level and no smoothing of the data. In the present analysis, the shallower feature is robust, appearing in all our test runs. The deeper feature is not, as its existence depends upon the chosen reference level and constraint set.

It also should be noted that the Lavin et al. (2003) DWBC estimate at $22 \times 10^6 \text{ m}^3 \text{ s}^{-1}$ was only half of ours. Rosón et al. (2002) in their calculation of meridional carbon transport employed the Lavin et al. circulation. Although the slightly different reference surfaces used in the two studies accounts for some of the differences in transport, the primary difference between the calculations is the velocity applied to the reference surface to obtain mass balance. Whereas the present study applies set of velocities (Fig. 7), Lavin et al. (2003) employed a single velocity within the Florida Straits and one other that was applied across the entire interior field.

3.3. Meridional TIC transport

The model also produces patterns of total inorganic carbon transport for the two cruises (Fig. 10, upper panels, and Fig. 11). The TIC transport profiles are similar in character to the complimentary mass transport figures. In the surface layers the transport through the Florida Straits is clear as is the large eddy feature near 70°W . In these upper layers, the net TIC transport

across the section is northward, but as in the case of mass, there is a net *interior* southward return flow. In the intermediate (AAIW and UCDW) layers the net transport is again northward and much, though certainly not all, of this poleward flow occurs in the Florida Straits. The net transport of deep TIC is southward, much of it carried by the DWBC. The transport of TIC closely follows that of mass because like density, the concentration of TIC changes little over the depth of the water column or basin extent (1998, mean TIC = $2173 \pm 29 \mu\text{mol kg}^{-1}$). This correspondence between the two properties affords us an opportunity to better understand our estimates of net TIC transport in light previous estimates (Table 4).

Given the large uncertainties, the new estimates are not significantly different from previous ones. The 1998 value of $-0.74 \pm 0.91 \text{ PgC yr}^{-1}$, does, however, suggest a smaller regional divergence in the meridional carbon transport than is suggested by either of the 1992 studies. Although the values are not significantly different, it is useful to understand why they are not identical. First, why does our 1992 estimate appear to be lower than the Rosón et al. (2002) value, second why is the 1998 estimate lower than either of the other 1992 values, and third why are the estimates of uncertainty so different?

3.3.1. The 1992 TIC transport estimates

Since the same data set was used to compute the 1992 estimates, any difference must be due to differing estimates of the velocity field. Approximately one-half of the difference can be attributed to the difference in net mass transport.

Three methods were found for producing TIC transports from our model similar to those of Rosón et al. (2002). The first was simply to constrain the model to do so. It is given that model should be able to meet this constraint as the range provided by the uncertainty on our estimate encompasses the Rosón et al. (2002) value. The model produces this stronger southward TIC transport by decreasing (from 4.6 to $2.4 \times 10^9 \text{ kg s}^{-1}$) the northward flux of water below 1000 db in the eastern basin which has a relatively high concentration of TIC, and by

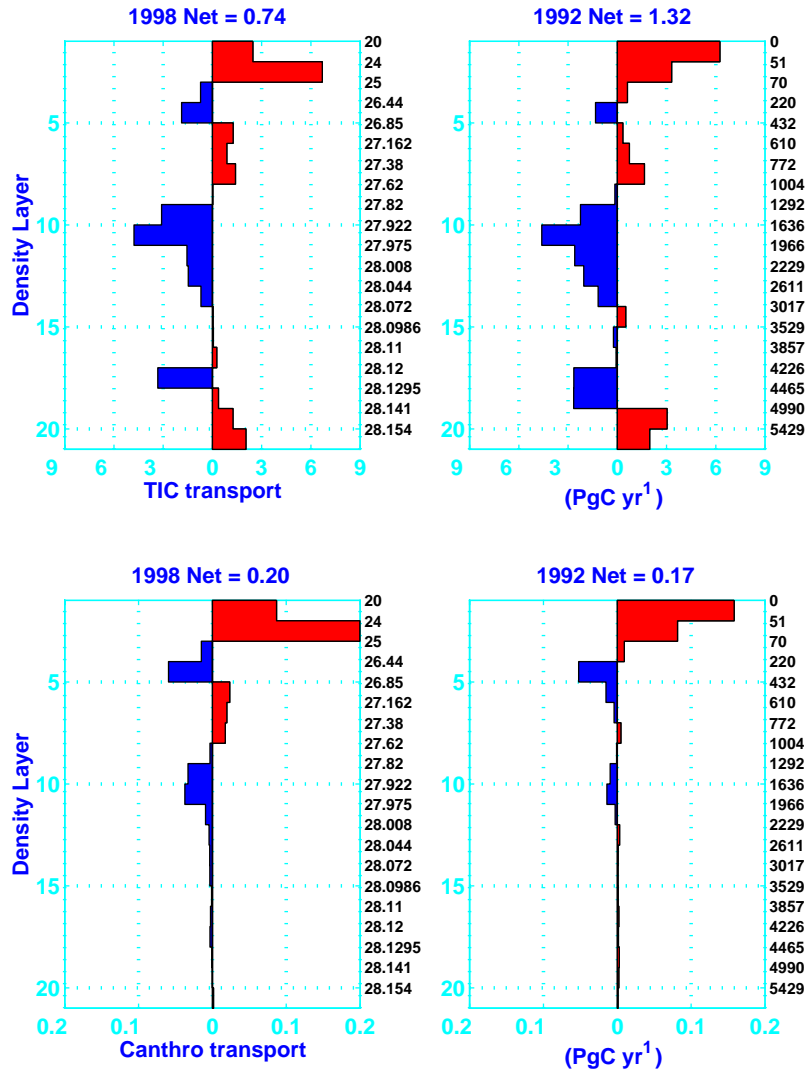


Fig. 10. Upper panels: the meridional total inorganic carbon transport profiles based on the 1998 (left-hand side) and 1992 (right-hand side) 24.5° model solutions. Lower panels: the same, for anthropogenic carbon. The right axis of the left-hand panels indicates the neutral density of each layer interface. The right axis of the right-hand panels indicates the average pressure of the layer interfaces in dbar. The net values given at the top of the panels is the net transport integrated from top to bottom. Positive values indicate northward flow.

decreasing the southward flow of deep water in the western basin which has lower TIC concentrations. Similar changes were found when a net zero or southward transport of silica was required across the section (the present model silica flux is $146 \pm 342 \text{ kmol s}^{-1}$). This balance between southward flow in the western basin, much of it carried in the DWBC, and northward flow of deep water

within the eastern basin is the same as that which controls the silica transport across this transect (Lavin et al., 2003).

The third manner in which a larger net southward TIC transport can be produced is to use the deep reference model that does not capture the deep western boundary current at all. Our conclusion, therefore, is that the likely reason for the

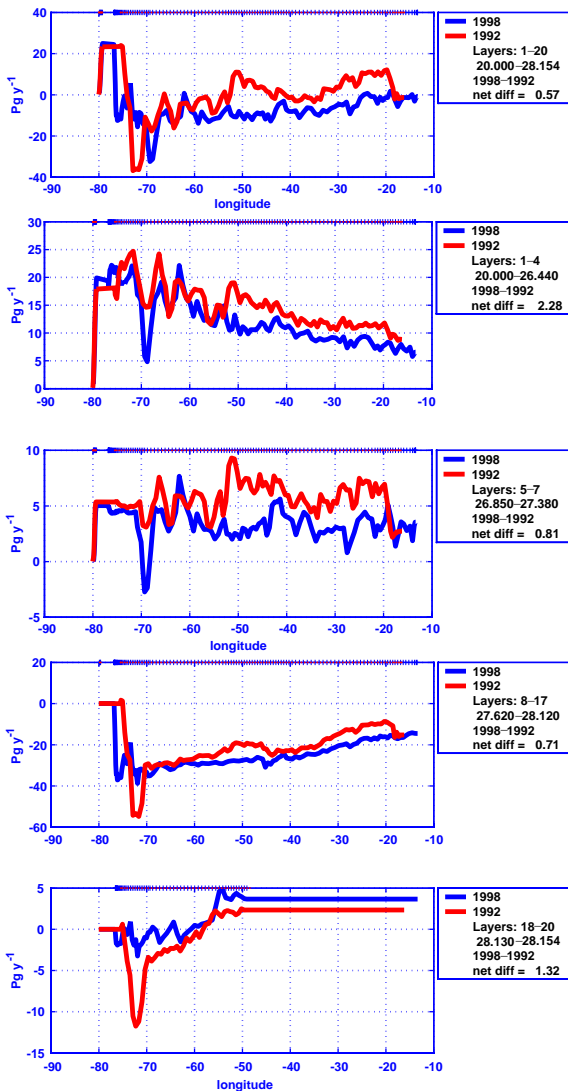


Fig. 11. A comparison of the cumulative inorganic carbon transport (including Ekman flow) for the 1998 (dark/blue) and 1992 (light/red) transects. The boxes to the right indicate the neutral density layers included in the integration (see Fig. 6), the difference in net transport between the two transects and the direction of the subtraction. The integration is performed from west to east. The lines at the top indicate the availability of data in the layer set for each station pair. Positive values indicate northward flow.

higher Rosón et al. (2002) TIC flux estimate is that their DBWC mass transport estimate is less than our own. The TIC flux estimates of both models could be improved through the integration of

available time series data in the far western basin as it becomes apparent that, at this latitude, it is necessary to fully resolve the DWBC to get the transport of TIC correct.

3.3.2. The 1998 versus the 1992 TIC transport estimate

Our 1992 and 1998 TIC transport estimates are based on similar models. Still it appears that differences in the velocity field, here resulting from the differing data, are the main cause of the difference in TIC transport estimates. About 15% of TIC transport difference is due to the difference in net mass transport. Separating the field into overturning components equal to the layer mean TIC concentrations times the layer transports, and gyre components equal to the difference between the net layer transports and the associated overturning components, shows that two-third of the TIC transport difference (0.4 PgC yr^{-1}) is due to differences in overturning. That is, although both transects carry a net overturn of $13\text{--}14 \times 10^9 \text{ kg s}^{-1}$, the 1992 transect carries more ($\sim -21.6 \times 10^9 \text{ kg s}^{-1}$) deep water rich in TIC southward than the 1998 transect ($\sim -17.6 \times 10^9 \text{ kg s}^{-1}$). The gyre components, which carry TIC northward, are responsible for the other third (0.2 PgC yr^{-1}).

These lower estimates of ocean TIC flux bring into question the concept that the tropical Atlantic is constantly outgassing carbon, while the sub-polar Atlantic is absorbing it (Fig. 12). Seasonal variations may be important, as we have already mentioned the strong correlation between upper layer temperatures and TIC; but circulation differences likely dominate, as the TIC transports are strongly correlated with the patterns and magnitude of mass transport.

3.3.3. The TIC transport uncertainty estimates

The uncertainty in the carbon transports are an issue as they are directly related to the uncertainty in mass transport. The uncertainty estimate for the TIC transport computed here come directly from the inverse model formulation (Wunsch, 1996). The solution, $\hat{\mathbf{b}}$ to Eq. (3) is

$$\hat{\mathbf{b}} = \mathbf{K}y \quad \text{and} \quad \mathbf{P} = \mathbf{R}_{xx} - \mathbf{KAR}_{xx}, \quad (4)$$

Table 4

Net transports of mass and other properties across the 24.5°N derived from the inverse model and compared to previous estimates

Property (units)	1998		1992		Rosón et al. (2002)		Brewer et al. (1989)	
MASS (10^9 kg s^{-1})	-1.0	± 0.9	-1.1	± 1.0	-1.3	—	-0.8	—
SALT (10^6 kg s^{-1})	-27.1	± 30.5	-26.8	± 34.0	-28.0	± 1.0	—	—
TIC (PgC yr^{-1})	-0.74	± 0.91	-1.32	± 0.99	-1.59	± 0.08	-1.21	—
$C \star_{\text{ANTH}}$ (PgC yr^{-1})	0.20	± 0.08	0.17	± 0.06	0.23	± 0.08	—	—

The Brewer et al. (1989) results are corrected to include the effect of the net mass transport from Bering Strait through flow and freshwater. Positive values are northward ($1 \text{ PgC yr}^{-1} = 2642 \text{ kmol Cs}^{-1}$).

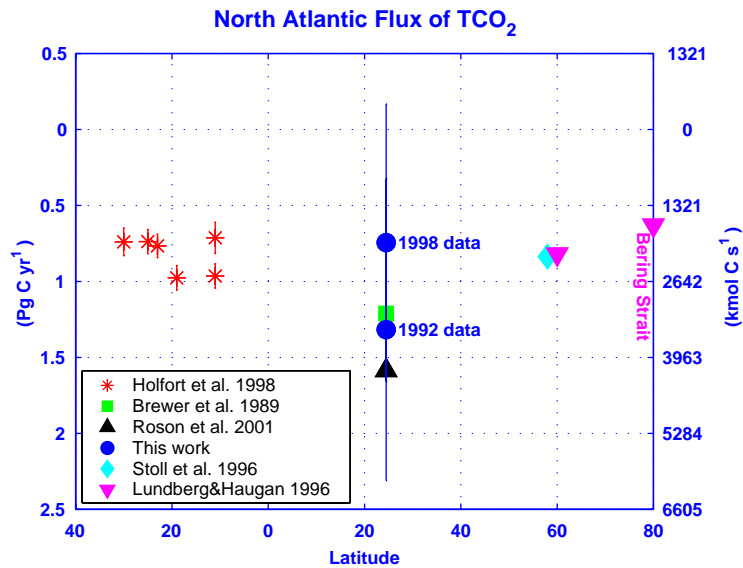


Fig. 12. Carbon transport as a function of latitude in the Atlantic (adapted from Wallace (2001) and updated with the results from this analysis).

where $\mathbf{K} = \mathbf{R}_{xx} \mathbf{A}^T (\mathbf{R}_m + \mathbf{A} \mathbf{R}_{xx}^{-1} \mathbf{A}^T)^{-1}$, \mathbf{R}_m is the a priori data covariance estimate, \mathbf{R}_{xx} is the a priori solution covariance estimate, and \mathbf{P} is the a posteriori solution covariance estimate about the unknown true values of the solution. \mathbf{P} is used to compute the uncertainty in the property transports (Macdonald, 1995) and so includes the various components of uncertainty described in Section 3.1.

The Rosón et al. (2002) TIC transport uncertainty estimate is computed by applying a perturbation of $\pm 2 \text{ Sv}$ to the interior transport field every 20 m and the opposite to the Florida Current to maintain the mass balance. This “transport error” is combined with a perturbation of $\pm 4 \mu\text{mol kg}^{-1}$ in TIC to produce the

$\pm 200 \text{ kmol s}^{-1}$ (0.08 PgC yr^{-1}) cited. This uncertainty is small compared to ours. The difference may arise from the Rosón et al. (2002) assumption of a perfect mass balance. Holfort et al. (1998) uses a completely different method. Taking a number of different inverse models that are solved using the SVD technique, they decide upon a range of ranks for which the carbon transport versus rank is fairly stable. The uncertainty is then taken to be the standard deviation across this range of ranks and models. Since this method is based upon the a priori choice of TIC transport range, it would appear to be self-limiting in terms of the magnitude of the a posteriori uncertainty estimate.

When our model was forced to meet the Rosón et al. (2002) estimate of TIC transport, their

estimate of uncertainty was also applied. This model was unable to produce the small uncertainty (0.08 PgC yr^{-1} , equivalent to a mass transport uncertainty $\sim 0.09 \times 10^9 \text{ kg s}^{-1}$) suggested by these previous studies (Holfort et al., 1998; Rosón et al., 2002). That is, these very small uncertainties are inconsistent with the observations and model physics. We therefore believe that the uncertainty estimates of Holfort et al. (1998) and Rosón et al. (2002) are unrealistically small. In the final section, we discuss what improvements can be made to the model to reduce the size of the error bars.

3.4. Meridional $C_{\text{★ANTH}}$ transport

Our analysis suggests a northward meridional transport of $C_{\text{★ANTH}}$ across 24.5°N of $0.20 \pm 0.08 \text{ PgC yr}^{-1}$ (1998) and $0.17 \pm 0.06 \text{ PgC yr}^{-1}$ (1992) (Table 4). These transport estimates and their uncertainties are consistent with both each other and with previous estimates, indicating that no observable temporal variation has taken place. This result would suggest that either no change has occurred or that the change over this 6-year period is too small to observe given the estimated uncertainties, and a longer period between transects may be necessary to observe $C_{\text{★ANTH}}$ transport variations. This issue is the same encountered with heat transport where changes in transport are too small to be observed in spite of significant warming from the surface to the deep Atlantic (Lavin, 1999).

Concentrations of $C_{\text{★ANTH}}$ are surface intensified, and although surface values are generally higher to the north of 24.5°N than to the south (Gruber, 1998), the surface to depth difference dominates. The transport weighted mean concentrations of $C_{\text{★ANTH}}$ are 56.7 and $38.6 \mu\text{mol kg}^{-1}$ for the 1998 Florida Current and interior data, respectively. Therefore, the net transport of $C_{\text{★ANTH}}$ across 24.5°N is strongly affected by the difference in concentrations between the northward flowing, relatively shallow Florida Current (carrying 0.7 PgC yr^{-1}) and the mass balancing interior return flow (carrying -0.4 PgC yr^{-1} in the western basin and -0.1 PgC yr^{-1} in the eastern basin). The high

transport weighted mean concentration of $C_{\text{★ANTH}}$ in the interior (high relative to the area averaged mean) indicates that higher concentrations of $C_{\text{★ANTH}}$ tend to be associated with higher transports, as in the DWBC for example.

It is of course important to be aware when looking at net meridional transports across basinwide sections, such as this one in the subtropical North Atlantic, that small net values are often the result of subtracting one very large number from another very large number. This is particularly true of TIC in the subtropical Atlantic, but is less true of $C_{\text{★ANTH}}$. Here in the 1998 transect, for example, this subtraction can be thought of as occurring:

- vertically within the meridional overturning cell: $13 \times 10^9 \text{ kg s}^{-1}$ mass transport associated with surface and intermediate waters traveling northward minus $18 \times 10^9 \text{ kg s}^{-1}$ deep southward flow plus $4 \times 10^9 \text{ kg s}^{-1}$ of bottom water moving to the north, resulting in a small southward net mass transport of only $-1 \times 10^9 \text{ kg s}^{-1}$. The TIC overturning cell is the sum of 10.1 PgC yr^{-1} northward flow of surface and intermediate water minus 14.5 PgC yr^{-1} deep flow plus 3.7 PgC yr^{-1} bottom water transport, resulting in a net transport of only -0.7 PgC yr^{-1} . The net flux is only 5% of the overturning components. For $C_{\text{★ANTH}}$ the overturning is composed of 0.3 PgC yr^{-1} in the upper layers balanced by 0.1 PgC yr^{-1} in the deep layers (there is no significant bottom water transport) for a net transport of 0.2 PgC yr^{-1} , a value that is of the same order of magnitude as the upper and lower limb components;
- or horizontally within the gyre: a strong surface intensified Florida Current carrying $31.4 \times 10^9 \text{ kg s}^{-1}$ northward, nearly balanced by an interior return flow of $-32.3 \times 10^9 \text{ kg s}^{-1}$ dominated by the wind-driven upper layers (Fig. 9, layers 1–4) and the DWBC (Fig. 9, layers 8–17). The associated carbon system shows 25 PgC yr^{-1} moving northward in the Florida Current, nearly balancing a return flow of 25.7 PgC yr^{-1} . The net flux value is only 3% of the component fluxes. Again for $C_{\text{★ANTH}}$ the story is different 0.7 PgC yr^{-1} flowing

northward in the boundary current and -0.5 PgC yr^{-1} returning in the interior.

Therefore, even as we estimate mean meridional carbon transports based on the previous success of such methods in estimating heat fluxes, serious consideration must be given to possible temporal variability in the large flows that we integrate across. Such variability could adversely affect our ability to accurately predict mean present day values, as well as possible future values. The C^{\star}_{ANTH} estimates should be less affected by this problem and, therefore, although C^{\star}_{ANTH} can be calculated only indirectly, it may be more appropriate to use than the directly measured TIC when looking for temporal variations.

4. Discussion

The net northward transport of C^{\star}_{ANTH} is opposite the net flow of total carbon and suggests, as has been found by others (Holfort et al., 1998; Rosón et al., 2002; Wallace, 2001), that in spite of today's greater atmospheric carbon levels, the pre-industrial southward transport of carbon within the Atlantic was stronger than it is today.

Taking the average of the 1998 and 1992 estimates¹ for the transport of TIC and C^{\star}_{ANTH} at 24°N , and values from the literature at 78°N (Lundberg and Haugan, 1996) and in the South Atlantic (Holfort et al., 1998), and keeping in mind the magnitude of the uncertainties, we explore how these estimates balance with the uptake from the atmosphere (Takahashi et al., 2002; Wanninkhof et al., 2001) and rivers, and provide estimates of carbon storage based on this balance (Fig. 13). The Takahashi et al. (2002) pCO_2 climatology used along with the NCEP 6-h winds as outlined in Wanninkhof et al. (2001) suggests that to the north of 24°N latitude the uptake of carbon from the atmosphere occurs at a rate of $22 \text{ gCyr}^{-1}\text{m}^{-2}$, to the south it suggests outgassing at rate of about $4 \text{ gCyr}^{-1}\text{m}^{-2}$. The storage of C^{\star}_{ANTH} appears to occur mainly to

¹Unless specifically indicated otherwise, 1992 refers to the present analysis of the 1992 transect.

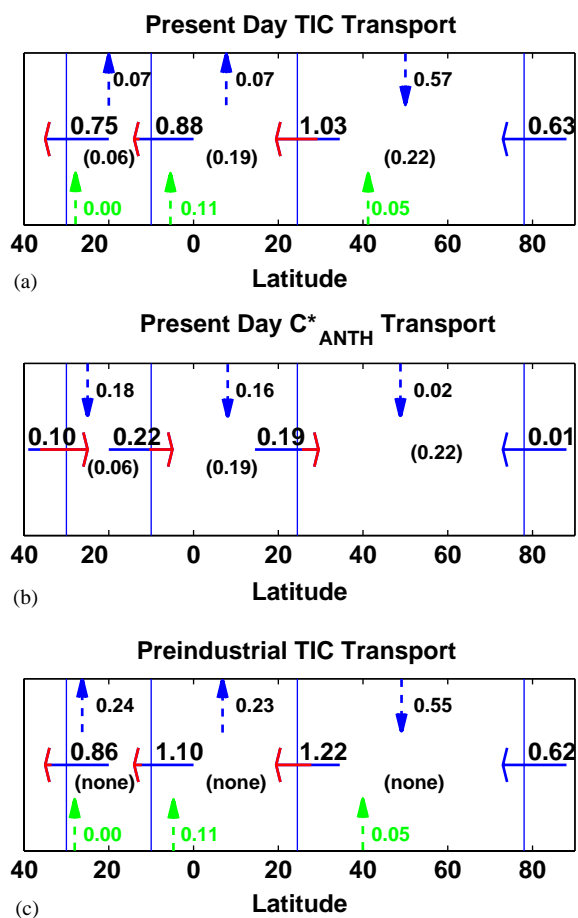


Fig. 13. (a) Estimates of present day total inorganic carbon transport (solid arrows) based on the average of the 1998 and 1992 model results, air/sea exchange (dark/blue dashed arrows) from monthly pCO_2 values (Takahashi et al., 2002) combined with gas exchange wind speed relationships using the monthly average and second moment to take the wind speed variability into account (Wanninkhof et al., 2001), river input (light/green dashed arrows) based on the river discharge estimates of Perry et al. (1996), taking the inorganic carbon concentration within the rivers to be order $1000 \mu\text{mol kg}^{-1}$ and assuming burial, respiration and outgassing of organic carbon occurs close to the ocean boundaries (Wallace, 2001; Aumont et al., 2001) and finally storage (in parentheses) which is computed as the residual of the other terms. The transport values across 10°S and 30°S are from Holfort et al. (1998). Those across 78°N are from Lundberg and Haugan (1996). (b) The same for present day C^{\star}_{ANTH} . Each air/sea flux estimate is the residual of the other values in the particular box. (c) The same for the pre-industrial Atlantic Ocean. The light grey/red portions of the oceanic transport arrows indicate the estimated uncertainty. Units are PgC yr^{-1} .

the north of 10°S in spite of the decrease in $C_{\text{★ANTH}}$ uptake with latitude. Uptake of $C_{\text{★ANTH}}$ per unit area between 78°N and 24°N is estimated at 1 gCyr⁻¹m⁻², between 24°N and 10°S at 6 gCyr⁻¹m⁻² and between 10°S and 20°S at 14 gCyr⁻¹m⁻².

The pre-industrial system is taken as the difference between the present day TIC and $C_{\text{★ANTH}}$ patterns, assuming that the biological conditions, riverine input of carbon and circulation have not changed. Prior to the industrial revolution, uptake of TIC to the north of 24°N was similar to that occurring today; however, there appears to have been a marked decrease in outgassing between 24°N and 30°S brought on by the uptake of anthropogenic carbon (Fig. 13c). The results suggest that the difference between today's carbon system and that which occurred prior to the burning of fossil fuels is brought about by today's uptake of anthropogenic carbon, which is stronger to the south and which is transported northward to be stored within the northern basin.

The storage of anthropogenic carbon is defined as the change over time of the depth integrated concentration of $C_{\text{★ANTH}}$.

$$\text{Storage of } C_{\text{★ANTH}} = \frac{d}{dt} \int C_{\text{★ANTH}} dz. \quad (5)$$

Using our $C_{\text{★ANTH}}$ estimates from the 1998 and 1992 transects to perform the integration, we obtain average specific inventories of 45±11 and 65±8 molC m⁻² at 24.5°N for the 1992 and 1998 data sets, respectively. As would be expected, these values tend to be larger than the 34±7 molC m⁻² estimated by Gruber (1998) based on a 1982 data set for the latitude band 18–27°N. In spite of the fairly large uncertainties, the three values taken together suggest a continued uptake and an increased storage of $C_{\text{★ANTH}}$ within the basin. Differencing the 98/92 mean specific inventories suggests a change over the 6-year period in the $C_{\text{★ANTH}}$ inventory at 24.5°N of 4.4±3.0 × 10⁻¹⁴ PgCyr⁻¹ m⁻². It is known that the specific inventory within the Atlantic increases with latitude (Gruber, 1998). Therefore, to obtain an estimate of the storage within the basin based upon these changes would require similar calcula-

tions performed at a number of different locations. Such work is part of an ongoing analysis.

Using the 1998 and 1992 repeat transects at 24.5°N in the Atlantic, we have investigated the details of total inorganic carbon and anthropogenic carbon fields and transports, and have looked at how they have changed over the period of time between the observations. We have determined a rate of increase in the surface CO₂ concentration from both fields of 1.5±0.6 μmol kg⁻¹ yr⁻¹, which is consistent with the estimate based on pCO₂ measurements. The transport of $C_{\text{★ANTH}}$ is northward and is of similar magnitude in the two sections. It is dominated by the difference in concentrations between the northward flowing shallow Florida Current and the interior return flow. The transport of TIC is southward. The TIC transport estimates are sensitive to the estimated mass transport of the DWBC.

One issue with the present model, which uses only a single transect and therefore cannot take full advantage of divergence and anomaly constraints, is the large uncertainty in the TIC transports. The uncertainties computed here can be decreased in future models by including early and late 1990s data from 48°N and 57°N, which will allow the use of constraints on phosphate/oxygen and nitrate/oxygen combinations, as well as the use of anomaly constraints that together should provide a stronger constraint set (Ganachaud, 1999) for producing direct estimates of TIC and $C_{\text{★ANTH}}$ transport and divergence. Although error bars on TIC transports as small as those suggested by previous authors appear unlikely, ongoing work suggests that a factor of two reduction in the magnitude of the uncertainties presented here can be expected. The new models will also allow direct estimations of storage and a residual calculation of air–sea CO₂ fluxes that can be compared to the estimates of Takahashi et al. (2002) used here.

The increased effort during the WOCE, OACES and JGOFS programs to directly measure carbon dioxide concentrations in seawater makes it possible to combine information from several basinwide transects in the North Atlantic to look at the large-scale transport and storage of CO₂. By

combining these modern, high resolution, hydrographic sections, we can gain insight into the global distribution of sources and sinks of CO₂, make an educated inference as to how these distributions separate into an historical background and an anthropogenic signal, and continue the compelling task of estimating how the buildup of fossil fuels in the atmosphere is reflected in the oceanic concentrations of CO₂.

Acknowledgements

This research was carried out in part under the auspices of the Cooperative Institute of Marine and Atmospheric Studies (CIMAS), a Joint Institute of the University of Miami and the National Oceanic and Atmospheric Administration, cooperative agreement #NA67RJ0149, and it is was funded by the Global Carbon Cycle Program of the National Oceanic and Atmospheric Administration Office of Global Programs and the Office of Oceanic and Atmospheric Research. We gratefully acknowledge the support of J. Toole and the National Science Foundation grant OCE-0079383, which allowed this work to be completed. We thank A. Lavín, G. Rosón, and M. Álvarez for supplying us with their 1992 anthropogenic carbon estimates as well as some of the details of their analysis of the 1992 A05 transect and J. Bullister for allowing us the use of the 1998 CFC data. We also acknowledge the time and effort given this manuscript by one internal and four external reviewers. This is U.S. JGOFS Contribution 967.

Appendix A. A method for calculation the anthropogenic CO₂

The TIC in the oceans is controlled by biological processes such as the production and remineralization of organic matter and calcium carbonate, and air–sea CO₂ exchange including anthropogenic CO₂. The technique to determine the anthropogenic CO₂ component is based on separating the influence of these processes on TIC concentrations. The method used here is a simplified

version of the one originally developed by Gruber et al. (1996), and is based on the same general concepts as earlier methods. This method introduces a quasi-conservative tracer, ΔC^{\star} , defined as

$$\begin{aligned} \Delta C^{\star} = & \text{TIC}^{\text{MEAS}} + R_{\text{C:O}}(\text{O}_2^{\text{EQ}} - \text{O}_2^{\text{MEAS}}) \\ & - 0.5[A_T^{\text{MEAS}} - A_T^0 - R_{\text{N:O}}(\text{O}_2^{\text{EQ}} - \text{O}_2^{\text{MEAS}})] \\ & - C^{\text{EQ}}(\text{fCO}_2 = 280 \mu\text{atm}, A_T^0, \theta, S), \end{aligned} \quad (\text{A.1})$$

where superscript “MEAS” refers to measured concentrations in water samples, O_2^{EQ} and O_2^{MEAS} are the saturation and in situ concentrations of oxygen, respectively, A_T^0 is the preformed alkalinity, A_T , that a subsurface water parcel had when it was last at the surface ocean, C^{EQ} is the TIC in equilibrium with the preindustrial atmosphere CO₂ fugacity of 280 μatm for the sample’s salinity (S), potential temperature (θ), and A_T^0 ; and $R_{\text{C:O}}$ and $R_{\text{N:O}}$ are the stoichiometric ratios relating inorganic carbon and nitrate changes to dissolved oxygen changes, respectively.

The A_T^0 of a subsurface water parcel is estimated from multilinear regression using the conservation tracers S and PO as independent variables (here $\text{PO} = \text{O}_2 - R_{\text{O}_2:\text{P}} \times \text{P}$). The measured alkalinity data used by Gruber et al. (1996) gave the following relationship

$$\begin{aligned} A_T^0(\mu\text{mol kg}^{-1}) = & 367.5 + 54.9S \\ & + 0.0074\text{PO}, \end{aligned} \quad (\text{A.2})$$

where S is on a practical salinity scale, and PO is in $\mu\text{mol kg}^{-1}$. The standard error of the estimated A_T^0 is $\pm 11 \mu\text{mol kg}^{-1}$. The use of an additional variable such as θ to fit surface alkalinity data does not reduce the uncertainty in Eq. (A.2).

The C^{EQ} was calculated from the estimated A_T^0 and $\text{fCO}_2 = 280 \mu\text{atm}$ using the dissociation constants for carbonic acid of Mehrbach et al. (1973) and other ancillary constants as recommended by Lee et al. (2000b) and linearized using a least-squares linear fit:

$$\begin{aligned} C^{\text{EQ}} = & 2082.8 - 9.0(\theta - 9) - 5.1(S - 35) \\ & + 0.78(A_T^0 - 2320). \end{aligned} \quad (\text{A.3})$$

The sum of the first three terms in Eq. (A.1) is the preformed TIC of a sample (C^0) when the

sample was at the surface. ΔC^* is the difference between C^0 and C^{EQ} . If the ocean takes up more anthropogenic CO_2 , values of ΔC^* would increase. This ΔC^* reflects the anthropogenic CO_2 (C^*_{ANTH}) and air–sea disequilibrium (ΔC^{DISEQ}) at the time when the sample lost contact with the atmosphere ($\Delta C^* = C^*_{ANTH} + \Delta C^{DISEQ}$).

To separate C^*_{ANTH} from ΔC^* , ΔC^{DISEQ} must be estimated. Determining the air–sea CO_2 disequilibrium has been problematic in estimating anthropogenic CO_2 in the ocean (Sabine et al., 2002). The method used here is to assume that for deep-ocean density surfaces where one can safely assume that there is no anthropogenic CO_2 , the air–sea disequilibrium is equivalent to ΔC^* . Therefore, in this study, the mean value of ΔC^* below 3500 db has been added to all samples to correct for air–sea disequilibrium.

References

- Aumont, O., Orr, J.C., Monfray, P., Ludwig, W., Amiotte-Suchet, P., Probst, J.-L., 2001. Riverine-drive interhemispheric transport of carbon. *Global Biogeochemical Cycles* 15, 393–405.
- Bates, N.R., Michaels, F., Knapp, A.H., 1996. Seasonal and interannual variability of oceanic carbon dioxide species at the U.S. JGOFS Bermuda Atlantic Time-series Study BATS site. *Deep-Sea Research II* 43, 347–383.
- Battle, M., Bender, M., Tans, P., White, J.W.C., Ellis, J.T., Conway, T., Francey, R.J., 2000. Global carbon sinks and their variability inferred from atmospheric O_2 and $\delta^{13}C$. *Science* 287, 2467–2470.
- Beining, P., Roether, W., 1996. Temporal evolution of CFC 11 and CFC 12 concentrations in the ocean interior. *Journal of Geophysical Research* 101, 16445–16464.
- Bretherton, F., Davis, R., Fandry, C., 1976. A technique for objective analysis and design of oceanographic experiments applied to MODE-73. *Deep-Sea Research* 23, 559–582.
- Brewer, P.G., Goyet, C., Dryssen, D., 1989. Carbon dioxide transport by ocean currents at 25°N latitude in the Atlantic Ocean. *Science* 246, 477–479.
- Chen, C.T., Millero, F., 1979. Gradual increase of oceanic CO_2 . *Nature* 277, 205–206.
- Coachman, L.K., Aagaard, K., 1988. Transports through the Bering Strait: annual and interannual variability. *Journal of Geophysical Research* 93, 15535–15539.
- Doney, S.C., Bullister, J.L., 1992. A chlorofluorocarbon section in the eastern North Atlantic. *Deep-Sea Research* 39, 1857–1883.
- Doney, S.C., Bullister, J.L., Wanninkhof, R., 1998. Climatic variability in upper ocean ventilation rates diagnosed using chlorofluorocarbons. *Geophysical Research Letters* 25, 1399–1402.
- Fillenbaum, E., Lee, T.N., Johns, W., Zantopp, R., 1997. Meridional heat transport variability at 26.5°N in the North Atlantic. *Journal of Physical Oceanography* 27 (1), 153–174.
- Fukimori, I., Wunsch, C., 1991. Efficient representation of the North Atlantic in the early 80's. An atlas. *Progress in Oceanography* 27, 1–110.
- Ganachaud, A.S., 1999. Large scale oceanic circulation and fluxes of freshwater, heat, nutrient and oxygen. Ph.D. Thesis, Massachusetts Institute of Technology/Woods Hole Oceanographic Institution Joint Program in Oceanography, Cambridge, MA, 266pp.
- Ganachaud, A., Wunsch, C., 2003. Large-Scale Ocean Heat and Freshwater Transports during the World Ocean Circulation Experiment. *Journal of Climate* 16, 696–705.
- Gruber, N., 1998. Anthropogenic CO_2 in the Atlantic Ocean. *Global Biogeochemical Cycles* 12 (1), 165–191.
- Gruber, N., Sarmiento, J.L., Stoker, T.F., 1996. An improved method for detecting anthropogenic CO_2 in the oceans. *Global Biogeochemical Cycles* 10 (4), 809–837.
- Hall, M.M., Bryden, H.L., 1982. Direct estimates and mechanisms of ocean heat transport. *Deep-Sea Research* 29, 339–359.
- Hellerman, S., Rosenstein, M., 1983. Normal monthly wind stress over the World Ocean with error estimates. *Journal of Physical Oceanography* 13, 1093–1104.
- Holfort, J., Johnson, K.M., Schneider, B., Siedler, G., Wallace, D.W.R., 1998. The meridional transport of dissolved inorganic carbon in the South Atlantic Ocean. *Global Biogeochemical Cycles* 12 (3), 479–499.
- IPCC, 2001. Climate change: the scientific basis. In: Joos, F., Ramirez-Rojas, A., Stone, J.M.R., Zillman, J. (Eds.), Contribution of Working Group I to the Third Assessment Report of the Intergovernmental Panel on Climate Change. Cambridge University Press, Cambridge, UK, New York, NY, USA, p. 83.
- Lavin, A., 1999. Fluxes, trends and decadal changes in the subtropical North Atlantic. Ph.D. Thesis, Universidad de Cantabria, Spain, 222pp.
- Lavin, A.M., Bryden, H.L., Parrilla, G., 2003. Mechanisms of heat, freshwater, oxygen and nutrient transports and budgets at 24.5°N in the subtropical North Atlantic. *Deep-Sea Research I* 50, 1099–1128.
- Lee, K., Wanninkhof, R., Feely, R.A., Millero, F.J., Peng, T., 2000a. Global relationships of total inorganic carbon with temperature and nitrate in surface seawater. *Global Biogeochemical Cycles* 14 (3), 979–994.
- Lee, K., Millero, F.J., Byrne, R.H., Feely, R.A., Wanninkhof, R., 2000b. The recommended dissociation constants for carbonic acid in seawater. *Geophysical Research Letters* 27 (2), 229–232.
- Lee, T.N., Johns, W.E., Zantopp, R.J., Fillenbaum, E.R., 1996. Moored observations of western boundary current variability and thermohaline circulation at 26.5°N in the subtropical North Atlantic. *Journal of Physical Oceanography* 26, 962–983.

- Lewis, E., Wallace, D.W.R., 1998. Program developed for CO₂ system calculations. ORNL/CDIAC-10. Carbon Dioxide Information Analysis Center, Oak Ridge National Laboratory, U.S. Department of Energy, Oak Ridge, Tennessee.
- Lundberg, L., Haugan, P.M., 1996. A Nordic Seas-Arctic Ocean carbon budget from volume flows and inorganic carbon data. *Global Biogeochemical Cycles* 10, 493–510.
- Macdonald, A.M., 1995. Oceanic fluxes of mass, heat and freshwater: A global estimate and perspective. Ph.D. Thesis, Massachusetts Institute of Technology/Woods Hole Oceanographic Institution Joint Program, Cambridge, MA, 326pp.
- Macdonald, A.M., 1998. The global ocean circulation: a hydrographic estimate and regional analysis. *Progress in Oceanography* 41, 281–382.
- Mecking, S., 2001. Spatial and temporal patterns of chlorofluorocarbons in the North Pacific thermocline: a data and modeling study. Ph.D. Thesis, University of Washington, Seattle, WA, 272pp.
- Mehrbach, C., Culbertson, C.H., Hawley, J.E., Pytkowicz, R.M., 1973. Measurements of apparent dissociation constants of carbonic acid in seawater at atmospheric pressure. *Limnology and Oceanography* 18, 897–907.
- Molinari, R.L., Fine, R.A., Wilson, W.D., Curry, R.G., Abell, J., McCartney, M.S., 1998. The arrival of recently formed Labrador Sea Water in the Deep Western Boundary Current at 26.5°N. *Geophysical Research Letters* 25 (13), 2249–2252.
- Orr, J.C., Maier-Reimer, E., Mikolajewicz, U., Monfray, P., Sarmiento, J.L., Toggweiler, J.R., Taylor, N.K., Palmer, J., Gruber, N., Sabine, C.L., Quéré, C.L., Key, R.M., Boutin, J., 2001. Estimates of anthropogenic carbon uptake from four three-dimensional global ocean models. *Global Biogeochemical Cycles* 15 (1), 43–60.
- Pérez, F.F., Álvarez, M., Ríos, A.F., 2002. Improvements on the back-calculation technique for estimating anthropogenic CO₂. *Deep-Sea Research I* 49, 859–875.
- Perry, G.D., Duffy, P.B., Miller, N.L., 1996. An extended data set of river discharges for validation of general circulation models. *Journal of Geophysical Research* 101 (D16), 21339–21349.
- Rintoul, S.R., Wunsch, C., 1991. Mass, heat, oxygen and nutrient fluxes and budgets in the North Atlantic Ocean. *Deep-Sea Research* 38 (Suppl. 1), s355–s377.
- Roach, A.T., Aagaard, K., Pease, C.H., Salo, S.A., Weingartner, T., Pavlov, V., Kulakov, M., 1995. Direct measurements of transport and waters properties through the Bering Strait. *Journal of Geophysical Research* 100, 18443–18457.
- Roemmich, D., Wunsch, C., 1985. Two transatlantic sections: meridional circulation and heat flux in the subtropical North Atlantic Ocean. *Deep-Sea Research* 32, 619–664.
- Rosón, G., Ríos, A.F., Lavín, A., Bryden, H.L., Pérez, F.F., 2002. Carbon distribution, fluxes and budgets in the subtropical North Atlantic. *Journal of Geophysical Research* 108, C5 (doi:10.1029/1999JC000047).
- Sabine, C.L., Key, R.M., Johnson, K.M., 1999. Anthropogenic CO₂ inventory in the Indian Ocean. *Global Biogeochemical Cycles* 13, 179–198.
- Sabine, C.L., Feely, R.A., Key, R.M., Bullister, J.L., Millero, F.J., Lee, K., Peng, T.-H., Tillbrook, B., Ono, T., Wong, C.S., 2002. Distribution of anthropogenic CO₂ in the Pacific Ocean. *Global Biogeochemical Cycles* 16 (4), 1083 (doi:10.1029/2001GB001369).
- Schimel, D., Alves, I., Heimann, M., Joos, F., Raymond, D., Wigley, T., 1996. CO₂ and the carbon cycle. In: Houghton, J.Y. (Ed.), *Climate Change 1995: The Science of Climate Change: Contribution of WGI to the Second Assessment Report of the IPCC*. Cambridge University Press, Cambridge, pp. 65–86.
- Schmitt, R.W., Bogden, P.S., Dorman, C.E., 1989. Evaporation minus precipitation and density fluxes for the North Atlantic. *Journal of Physical Oceanography* 19, 1208–1221.
- Siegenthaler, U., Sarmiento, J., 1993. Atmospheric carbon dioxide and the ocean. *Nature* 365, 119–125.
- Takahashi, T., Sutherland, S.G., Sweeney, C., Poisson, A.P., Metzl, N., Tilbrook, B., Bates, N.R., Wanninkhof, R., Feely, R.A., Sabine, C.L., Olafsson, J., Nojiri, Y., 2002. Global sea–air CO₂ flux based on climatological surface ocean pCO₂, and seasonal biological and temperature effects. *Deep-Sea Research II* 49, 1601–1622.
- Wallace, D.W.R., 2001. Storage and transport of excess CO₂ in the oceans: the JGOFS/WOCE global CO₂ survey. In: G. Siedler, J.C. Gould, Jr. (Eds.), *Ocean Circulation and Climate*. Academic Press, New York, pp. 489–521.
- Wanninkhof, R., Doney, S.C., Takahashi, T., McGillis, W.R., 2001. The effect of using time-averaged winds on regional air–sea CO₂ fluxes. In: Donelan, M., Drennan, W., Saltzman, E., Wanninkhof, R. (Eds.), *Gas Transfer at Water Surfaces*, *Geophysical Monograph*, Vol. 127. AGU, Washington, DC, pp. 351–357.
- Wanninkhof, R., Peng, T.H., Huss, B., Sabine, C.L., Lee, K., 2003. Comparison of inorganic carbon system parameters measured in the Atlantic Ocean from 1990 to 1998 and recommended adjustments. Technical Report, CDIAC, Oak Ridge, 45pp.
- Warner, M.J., Bullister, J.L., Wisegarver, D.P., Gammon, R.H., Weiss, R.F., 1996. Basin-wide distributions of chlorofluorocarbons CFC-11 and CFC-12 in the North Pacific: 1985–1989. *Journal of Geophysical Research* 101, 20525–20542.
- Wunsch, C., 1978. The general circulation of the North Atlantic west of 50°W determined from inverse methods. *Reviews in Geophysics* 16, 583–620.
- Wunsch, C., 1996. *The Ocean Circulation Inverse Problem*. Cambridge University Press, Cambridge, 442pp.